# Ingestible Electronics for High Quality Gastric Neural Recordings

By

Adam Matthew Gierlach

B.A.Sc., University of Toronto (2021)

Submitted to the Department of Electrical Engineering and Computer Science in Partial
Fulfillment of the Requirements for the Degree of

Master of Science

at the

MASSACHUSETTS INSTITUTE OF TECHNOLOGY

June 2023

| | |
|---|---|
| Authored by: | Adam Matthew Gierlach<br>Department of Electrical Engineering and Computer Science<br>May 18, 2023 |
| Certified by: | Carlo Giovanni Traverso<br>Associate Professor of Mechanical Engineering<br>Thesis Supervisor |
| Certified by: | Anantha P. Chandrakasan<br>Vannevar Bush Professor of Electrical Engineering and Computer Science<br>Thesis Supervisor |
| Accepted by: | Leslie A. Kolodziejski<br>Professor of Electrical Engineering and Computer Science<br>Chair, Department Committee of Graduate Students |

# Ingestible Electronics for High Quality Gastric Neural Recordings

By

Adam Matthew Gierlach

Submitted to the Department of Electrical Engineering and Computer Science
on May 18th, 2023 in Partial Fulfillment of the
Requirements for the Degree of
Master of Science

# Abstract

Recent advances in understanding the gut-brain axis, functional gastrointestinal disorders, and gastric stimulation therapies have highlighted the importance of the electrical signals that regulate the gastrointestinal (GI) tract. Current systems for measuring neural signals from the GI tract involve acute, invasive procedures that change the underlying electrical behaviors or cutaneous recordings which measure highly attenuated signals. This thesis describes the development of a non-invasive device for long term gastric recordings in freely moving patients known as Multimodal Electrophysiology via Ingestible Gastric Untethered Tracking (MiGUT). The custom device and electrodes are designed to conform to the stomach wall, wirelessly transmit high quality signals, all while fitting in an ingestible form capable of being easily delivered into the GI tract. MiGUT is shown to record the gastric slow wave *in-vivo* in pigs, along with signals that align with the heart and respiratory rate, and measure the expected response to prokinetic therapeutics. Multi-day measurements were obtained using MiGUT in a freely moving pig, recording changes in the slow wave during different behaviors with no artifacts observed during ingestion or movement. This type of data could enable a new level of understanding of one's GI tract, for health tracking and personalized diagnostics.

Thesis Supervisor: Carlo Giovanni Traverso
Title: Associate Professor of Mechanical Engineering

Thesis Supervisor: Anantha P. Chandrakasan
Title: Vannevar Bush Professor of Electrical Engineering and Computer Science

# Acknowledgments

First and foremost, I would like to thank Professor Giovanni Traverso and Professor Anantha Chandrakasan for giving me the opportunity to pursue this work with unparalleled guidance and support. Their vision and humble genius inspired me to grow, do my best work, and strive to create innovations that will change the world. They enabled all the work in this thesis. I am thrilled to continue my Ph.D. journey under their supervision and I excitedly look forward to what comes next.

I would like to thank Dr. Sean You for his mentorship and expertise that led to this project being such a success. With his modest brilliance, he continually elevated my research abilities while I was working alongside him and he also cooked up some amazing BBQ. He is also to thank for all the pig illustrations in this thesis. To the Novo Nordisk team old and new, I am grateful for the resources and expertise which made this research possible.

Thank you to our amazing animal team and technicians who seem to effortlessly provide all the supports which allowed this research to thrive. None of this would have been possible without Keiko, Josh, Wiam, and Alison who provided their exceptional skills with our colony of pigs. Thank you to Matt and Seokkee for making hundreds of 3D printed cases for us. I am also extremely grateful for the electrical technicians, specifically George who continued to keep the project alive until I returned after my internship and Injoo for help with device assembly. I must thank Dr. Hen-Wei Huang and So-Yoon for their electrical engineering insights, Dr. Miguel Jimenez on how to manage multiple projects more effectively, and Dr. Gary W. Liu for adding some humor to every conversation.

I would also like to thank my fellow graduate students and the many lab members across MIT and Brigham Women's Hospital. Thanks to everyone in the DARPA ADAPTER team for countless learnings about device integration. A special thanks to Jimmy and Dr. Ceara Byrne for making our late night brainstorming sessions entertaining. To the past and present members of the Anantha group who continue to teach me new things about circuit design and excite me about the work to come. To Louie for all the ski adventures which kept me sane outside the lab. To Anita, Dr. Jong Seung Lee, Patricia, and Dr. Stephanie Owyang for many adventures and stories to tell. To Deniz, Eunseok, Rishabh, and Kyungmi who kept the spark going at our lab socials. To Katherine, Tara, Vanessa, Jessie-Leigh, Katey, and Yuvie for keeping everything behind the scenes running smoothly. And of course, to all my fellow Canadians in the MIT Canadians Club.

I am especially grateful to all my past supervisors and cheerleaders. To Dr. Azadeh Kushki for being the first to springboard me into biomedical research. To Dr. Taufik Valiante and Prof. Roman Genov for introducing me to the world of neuroelectronics and showing me the beauty of the brain. To Dr. Gerard O'Leary for forming me into the researcher I am today and for being an amazing role model and an extraordinary researcher. To Dr. Kathryn McIntosh for her contagious passion for research.

Finally, thank you to my parents and family for supporting me throughout this journey and always providing new perspectives. Especially to my brother Matthew for his unwavering energy and confidence, with an unbreakable bear hug every time I return home.

# Contents

# List of Figures

# List of Tables

# Chapter 1 Introduction

Functional gastrointestinal (GI) disorders affect more than 40% of people worldwide [1], which frequently causes debilitating nausea, abdominal pain, and weight loss, with severe disease resulting in poor nutrition and unintentional weight loss [2]. These disorders, which by definition are abnormalities in the absence of any structural or biochemical findings, present as a complex combination of symptoms unique to each patient and can arise idiopathically or as a complication of other disorders [3]–[5]. This results in a lengthy diagnostic process trialing different therapeutics until the patients' symptoms are best resolved [5], [6]. More personalized diagnostic tools are required to determine the underlying cause and lead to faster, objective driven diagnosis.

Just like how doctors commonly use EKGs and EEGs to diagnose patients with electrical dysfunctions in the heart and brain, there are millions of neurons and associated electrically active cells in the GI tract which control motility, nutrient handling, immune responses and more [7]. However, these signals are poorly understood as clinicians and scientists do not have the tools to effectively monitor these slowly oscillating signals deep within the GI tract for long periods of time. While pioneering work has led to important discoveries from acute, highly invasive measurements, there is still much to be learned from long term recordings as the gut changes on a number of timescales; operating over hours to regulate motility, days depending what meals are ingested, and over the course of months depending on diet and the microbiome [8]. Thus, the ideal clinical system would provide high quality recordings for long periods of time while being easy to deploy as a diagnostic test.

## 1.1 Thesis Outline

This thesis is organized as follows:

- Chapter 1 provides background and context for the proceeding chapters. First, a brief review on neural activity in the gut is presented to understand how this all started, what to expect when measuring electrical signals in the gut, and what changes in disease states. Then the different types of medical devices available to record these signals are shown in context of their targeted use case and their drawbacks.

- Chapter 2 presents the development of an ingestible device for wireless, high quality biopotential recordings known as MiGUT, for Multimodal Electrophysiology via Ingestible Gastric Untethered Tracking. The design consideration of an ingestible device is first introduced. Custom conformal electrodes manufactured in the cleanroom are then described, tested in-vivo, and reviewed to inform the final electrode choice. These interface with a newly designed electronics system to wirelessly transmit measurements for long periods of time.

- In Chapter 3, validation of MiGUT is confirmed in anesthetized animals. The device is shown to be safely delivered endoscopically and record signals from the stomach and multiple nearby organs. Data processing and other control experiments are also outlined.

- Chapter 4 demonstrates the new wireless recording capabilities of MiGUT in untethered, freely moving animals which can be quickly and noninvasively administered. An initial analysis of the recorded data is presented.

- Chapter 5 will conclude the thesis by discussing the results in comparison to previous studies. Future directions and insights into additional studies are postulated.

The following sections that complete this chapter will reveal how electrical signals control your gut, and the challenges present in trying to measure these signals deep within you.

## 1.2 Neural Activity in the Gut

The Enteric Nervous System (ENS) is comprised of 400 to 600 million neurons spread throughout the GI tract and works with the Central Nervous System (CNS) to control the behavior of various gastric regions [7]. While the measurements from the ENS were first seen over a century ago, advances in acquisition systems and methodologies have only recently enabled a better understanding of normal and pathological behaviors, with additional interest growing in understanding the gut-brain axis.

### 1.2.1 History

The first set of experiments presenting the gastric slow wave were performed in 1921 by Walter Alvarez by placing electrodes on the abdominal wall of a woman so thin Alvarez could see her gastric contractions around three cycles per minute [9], [10]. Additionally, around this

time I. Harrison Tumpeer and R. C. Davis independently also reported of the electrogastrogram (EGG) signals, from different patient populations and using different recording techniques [11]–[13]. Throughout the late 1900s, more validation studies were conducted solidifying the existence of these signals at a large scale [14], with multiple studies building to the conclusion that these signals were unique pacemakers of the gastrointestinal tract which controlled the frequency of peristaltic contractions in the stomach [15]–[18]. Since then, advances in electrode technology, signal processing, and study design led by Lammers, O'Grady, Kelly, Du, and more have led to a more complete understanding of the electrical activity in the gut.

## 1.2.2 Physiological and Pathological Behaviors

The major components of the GI tract consist of the esophagus, stomach, small and large intestines, and anus, each of which have their own characteristic electrical behaviors. We will focus on the stomach as it has been the most well studied and clinically relevant, but the key components are recently starting to be analyzed in the intestines [19] and esophagus [20]. The stomach is responsible for accommodating (growing in size) to accept food, churning the food for easier digestion by means of peristaltic waves (Fed Motor Pattern), and emptying in a series of complex contractions driven by the Migrating Motor Complex (MMC) [21].

Normal behavior in the human stomach revolves around the proper generation of the slow wave, originating from pacemaker Interstitial Cells of Cajal (ICC) [21]. Waves in the pacemaker region of humans have been recorded at a frequency of approximately 3 cycles per minute (cpm) traveling with a velocity of 8mm/s with an amplitude of 0.57mV [22]. These waves propagate circumferentially down the corpus at a velocity of ~3mm/s, faster in the greater curvature to stay in phase with the lesser curvature, and decrease in amplitude to 0.25mV. Waves traveling up towards the fundus quickly slow and attenuate [22]. These waves are ever present but below the threshold voltage required to elicit peristaltic waves, which only occur when spiking activity is superimposed on the slow wave to surpass the required threshold voltage [21]. Waves in the antrum are more complex, and rapidly accelerate to 5.7mm/s with an increased amplitude of 0.52mV. These results from a fasted patient under anesthesia are supplemented by implanted electrodes showing similar results [23]–[25]. In orchestration with feedback networks from other neural pathways [7], these slow waves and generated spike potentials control the peristaltic waves that break up food and empty the stomach.

Pathological behaviors in the stomach have historically been investigated through the lens of slow wave frequency in mirroring analysis from the heart. Tachygastria is defined as abnormally high frequency of the slow wave (3.7-10cpm), while an abnormally low frequency corresponds with Bradygastria (0-2.5cpm) [10]. These abnormal slow wave frequencies have been shown to strongly correlate with loss of ICC pacemaker cells [26]. However non-invasive wearable tools for measuring the slow wave frequency have yet to be widely adopted due to limited diagnostic understanding [27]. To go beyond frequency analysis, O'Grady et al. used their high resolution mapping technique to spatially map the stomach of patients with gastroparesis, finding various abnormal initiation and abnormal conduction events [28]. While more research is still required, this supports a more intimate understanding of the stomachs state could better diagnose different gastric neuropathies; similar to how single channel EKGs are acceptable for fitness trackers to identify when something is wrong, and diagnostics typically requires multiple channel EKGs.

### 1.2.3 The Gut-Brain Axis

In addition to acute measurements of the pacemaker region and slow waves, fundamental research around the gut-brain axis would benefit greatly from long term measurements. This connection with the brain has been reported in patients with Parkinson's disease who present with GI motility issues before cognitive symptoms arise [29]–[31], and many with autism spectrum disorder present with gastrointestinal issues [32], [33]. Biopotential measurements tracking organ level changes may eventually be used to infer changes in the microbiome and other but-brain interactions.

## 1.3 Medical Devices for Gastric Recording

A number of new systems and devices have been created to enable the study of biopotentials in the GI tract. These can be subdivided into tethered, implantable, and wearable devices.

### 1.3.1 Tethered Systems

Tethered systems involve directly connecting the recording electrodes to an external acquisition system using long cables. By decoupling the electrodes and recording device, thus

removing the size and power requirements, this has enabled a number of high channel count, high resolution studies to be conducted. Two standout systems are those used by Lammers and O'Grady. Lammers et al. were the first to do high resolution mapping and recorded 240 channels using an 8-bit 1kSPS recording system designed for recording myocardial signals, connected to custom fabricated silver wire electrodes (0.3mm diameter in a 15x16 grid with 1mm spacing) in rabbits [34]. Inspired by this, O'Grady et al. recorded 192 channels in humans using an ActiveTwo System (Biosemi, Amsterdam, The Netherlands) sampling at 512SPS, with multiple gold electrodes in a 4x8 array spaced 7.6mm apart [22]. The gold electrodes were compared to Lammers silver wire electrodes and found to give comparable results [35]. Through these systems, the origin and propagation of the gastric slow wave has been thoroughly described in the healthy and pathologic human stomach [22], [28], and throughout large animal models [19], [34], [36], [37].

However, these systems come at the cost of invasiveness and provide only acute recordings during an operation. In [22] and [28] patients volunteered for this study as they underwent elective surgery, but it is unlikely an operation could be as a standard diagnostic test. Additionally, while in the aforementioned studies great care was taken to ensure minimal movement of the organs, it has been shown that movement can cause abnormal behaviors likely due to activating stretch receptors [36]. The operating room setting may have also resulted in abnormal recordings due to the surgery preparations. Specifically, as patients fast prior to surgery, behaviors such as the migrating motor complex and peristaltic waves may be altered. Lastly, there are conflicting viewpoints on the effect of anesthesia, with the majority agreeing it slightly to significantly diminishes the slow wave [38]. Overall, more data is still required to comprehensively address the impact of these limitations.

To overcome these challenges, Angeli et al. developed a high resolution mapping device that can record from the mucosa using endoscopic intubation [37]. This used the Constellation™ mapping catheter (Boston Scientific, Marlborough, MA, USA) to record from eight rings of eight electrodes spaced 7mm apart, and the same acquisition system as previously used by O'Grady [22], [37]. This study highlighted that recordings from the mucosa are comparable to those recorded from the serosa. Other groups have since shown mucosal recordings from ambulating patients, but these are limited in the number of electrodes and required nasally clipped leads

passed up the esophagus [23], [39]. While in the right direction, these tethered systems do not allow the patient to go about their daily lives for long periods of time.

## 1.3.2 Implantable Devices

To gather data before and after eating, implantable devices have been developed to record biopotentials over longer periods of time. In humans, the majority of data comes from Gastric Electrical Stimulator (GES) devices with recording channels [24], [25], [40]. For power efficiency, these devices typically sample at much slower rates with fewer channels; in [24] samples were recorded at 60SPS using a 12bit analog to digital converter from four channels. These studies have enabled recordings to be taken over multiple days while patients go about their daily lives but require invasive surgical placement. Other devices by [41]–[44] have also been developed for research, but these devices are quite large and have other tradeoffs (further discussed in Section 2.3.6).

## 1.3.3 Wearable Devices

Since the discovery by Alvarez using surface electrodes, the quality of electrogastrography (EGG) recordings have significantly improved but have yet to find their place in the standard diagnostic procedure [27]. The key challenge of these wearable systems is recording the heavily attenuated signal (by the abdomen) and minimizing artifacts from respiration and motion [45]. A number of signal processing techniques have been developed to recover the low amplitude slow waves while also removing motion artifacts [46], [47], but the best recordings still come from immobilized patients. To assist in these efforts, new multi-channel EGG systems have been shown to reveal the slow wave direction and speed in addition to frequency when coupled with advanced signal processing [48], [49]. However the quality of the recorded data still prevents widespread adoption.

# Chapter 2 Development of an Ingestible Device for High Quality Neural Recordings

Here we present the development of an ingestible device for Multimodal electrophysiology via Ingestible, Gastric, Untethered Tracking (MiGUT). First the design considerations are presented, followed by the development of conformal electrodes for neural recording in the stomach, then the design and validation of low power, wireless electronics.

## 2.1 Design Considerations

### 2.1.1 Opportunities for Ingestible Devices

Ingestible devices offer a noninvasive way to access signals deep within the body from the gastrointestinal tract. Endoscopic techniques are an important tool for visually evaluating the GI tract [50], with new endoscopic tools enabling more advanced tests and procedures such as photoacoustic and ultrasound imaging [51], laser therapy [52], and more. Ingestible devices could be designed to achieve the same level of biomarker tracking and/or therapy while also being less invasive than endoscopy (typically requiring sedation [53]). This has been proven in devices such as the FDA Cleared Medtronic PillCam which provides good visualization of the colon without the drawbacks associated with endoscopy [54]. Since this first adoption and acceptance of ingestible devices clinically, other ingestible devices have been designed with different sensing modalities such as pH, temperature, pressure, bacterial and gas sensing, ultrasonic imaging, and modulation devices [55]–[60]. In addition to studying the gastrointestinal tract, ingestible devices boarder or transit within close proximity of other key organs, which could provide an effective avenue for high fidelity measurements or targeted therapies. This could enable a no instructions needed diagnostic tools to be easily deployed in or shipped to each person's home someday.

### 2.1.2 Key Challenges

There are a few fundamental challenges and constraints to consider when designing ingestible, especially relating to size, communication, power, and interface.

The biggest challenge with ingestible devices is size. The goal is to pack as much function and power into the device while allowing it to still be safely ingested and pass through the GI tract. Currently the largest standard pill size used is the 000 ("triple zero") capsule with a diameter of 9.91mm and a length of 26mm. However, these gelatin capsules usually dissolve to release their therapeutic. Passage studies of various capsule sizes show in order to ensure a there is minimal risk of blockage, which constitutes a life threatening complication, a device should have its longest dimension be no more than 15.5mm [61]. This is a challenge with ingestible devices, which typically carry onboard batteries for power, large antennas, and electronic circuitry; the PillCam which measures ⌀11x26mm is retained at a rate of 1.4% [57], [62]. While no studies have been done on device roughness, it is generally desirable for devices to be smooth and not cut inner tissues. However, case studies have revealed ingestion of razor blades can pass safely without intervention [63], indicating deviations from standard circular pill shapes to those more accommodating for packing dense electronics may be acceptable.

Closely related to size is power, specifically power density. While implantable devices such as neurostimulators or pace makers use lithium-based batteries, these are very large and not amenable to an ingestible form factor [64]. Most ingestibles on the market use Silver-Oxide ($AgO_2$) batteries for their safety and typically contain higher power density than lithium-ion batteries [65]. However, $AgO_2$ batteries are not typically suited to drive the high current consumption required for wireless communication. Lithium-ion batteries are convenient for their ability to be recharged and provide high levels of sustained current but are typically considered too volatile if there is a concern of gastric fluid leakage into the device. Battery packaging also needs to be considered for overall size optimization. While this is an active area of research, future devices will likely rely on wireless power solutions or wireless charging to ensure long term use.

Wireless communication methods for implantable and ingestible devices include piezo electric (ultrasound), radio frequency, optical, and magnetic modalities [65]. However the environment of the GI tract is much deeper, with more diverse tissue layers between the device and the receiver. This creates issues relating to penetration depth of different radio wave frequencies [66], while other communication methods typically require bulky external receivers. Current ingestible devices compromise by using sub 1-GHz radio frequencies, specifically in the

ISM band (433MHz or 915MHz) [57], although recent devices have been shown to successfully implement Bluetooth (2.4GHz) communication with careful antenna tuning [67].

Finally a stable interface is required to make the device meaningful. Rigid electronics and electrodes limit their size as the gastrointestinal tract consists of many folds and is in motion [7]. Current tethered devices use flexible electrodes, but these have only been extensively tested on the serosa [38]. Electrodes for interfacing with the mucosa have typically been individual wire electrodes secured to the mucosa with clips or pressed against the mucosa using a balloon [23], [37], [39]. Additionally, the electrodes should be of inert material which does not react with the gastric environment that has a wide pH range (pH of 2.1 in the fasted state or 3-7 while fed in the stomach, which can be different in the upper and lower stomach, and increasing pH in the intestines [65]) and contains many other harsh digestive compounds.

## 2.1.3 Design Decisions

Considering the above challenges and current implementations for mitigating them, the following initial design decisions were formed:

- **PillCam or smaller device dimensions** to ensure a future path for clinical translation should be met. Specifically, a maximum diameter of 11mm and length of 26mm or smaller [57], allowing for flexibility in using off the shelf components. Further miniaturization, specifically such that the maximum dimension is under 15.5mm, will be outlined in Section 5.2.
- **Li-ion battery power** will be used for flexibility in device design and ease of use for later data gathering stages (allowing for recharging and reuse of the device while providing a path for wireless charging to increase recording length). Powering with Silver Oxide batteries must be demonstrated to ensure safety of future devices but does not have to be implemented in this version.
- **915MHz communication** will be used as it has been proven as a robust communication method in commercially used ingestibles [56], [57].
- **Custom flexible electrodes** will be designed discussed in Section 2.2.

## 2.2 Conformal Electrodes for Neural Recordings

To acquire neural signals from the gastrointestinal tract, a number of strategies have been taken. While wireless measurements using Magnetic Resonance Imaging (MRI) [68], [69] and optogenetics [70] have been previously reported, the best results come from metal electrodes measuring the electrical signals directly. MRI is limited to measuring contractions and has resolution limits impeding study of complex behaviors [71], while optogenetics are not translatable to humans. In contrast, metal electrodes can be used for long term recordings and have been used in many pacemakers and neurostimulators with minimal complications. The current challenges with metal electrodes revolve around maintaining a stable interface to ensure high quality recordings in the environment of the GI tract.

### 2.2.1 Micron Thick Conformal Electrodes

In comparing current electrode designs, a multi electrode array arrangement is seen to be the most valuable arrangement – enabling the analysis of slow wave direction and velocity. However the current solutions, even ones made from flexible substrates, still remain relatively stiff as the size grows to accommodate a larger grid of electrodes. In experiments, wet gauze to be placed over the electrodes is commonly used to ensure good contact (in addition to ensuring the interface does not dry) [22]. We hypothesized by removing the thickness in the z-dimension, large electrode arrays could more effectively conform to the surface of the mucosa.

Multiple sixteen-channel electrodes were designed as shown in Figure 2.2.1, with varying degrees of electrode size (5μm to 200μm diameter) and electrode spacing (pitch spanning 200μm to 4mm). Specifically, to test the impact of electrode size one design incorporated four electrodes with exposed pads of diameter 5μm, 30μm, 80μm and 180μm (cut out 10μm smaller than actual electrode size on all sides for mechanical stability) with a pitch of 200μm (Figure 2.2.1A). Another small electrode design fabricated was inspired from neural multi electrode arrays was a 4x4 grid of 30μm diameter electrodes with a pitch of 200μm (Multichannel Systems GmbH, BW, Germany). Most other electrodes were designed to sweep the pitch from 1mm to 4mm with varying grid arrangements, since the slow wave spans much greater distances. To interface with different recording systems, contacts were placed with 0.5mm pitch to allow for mating with Flat Flexible Cable (FFC) connectors. To assist with the flexibility, it was

hypothesized adding 20µm diameter holes with a pitch of 100µm to 200µm would allow for additional flexibility and were added to some designs (Figure 2.2.1A). Additionally, some designs included a pivot point and/or ninety-degree rotation from the connector side to decouple movements from the connector side.
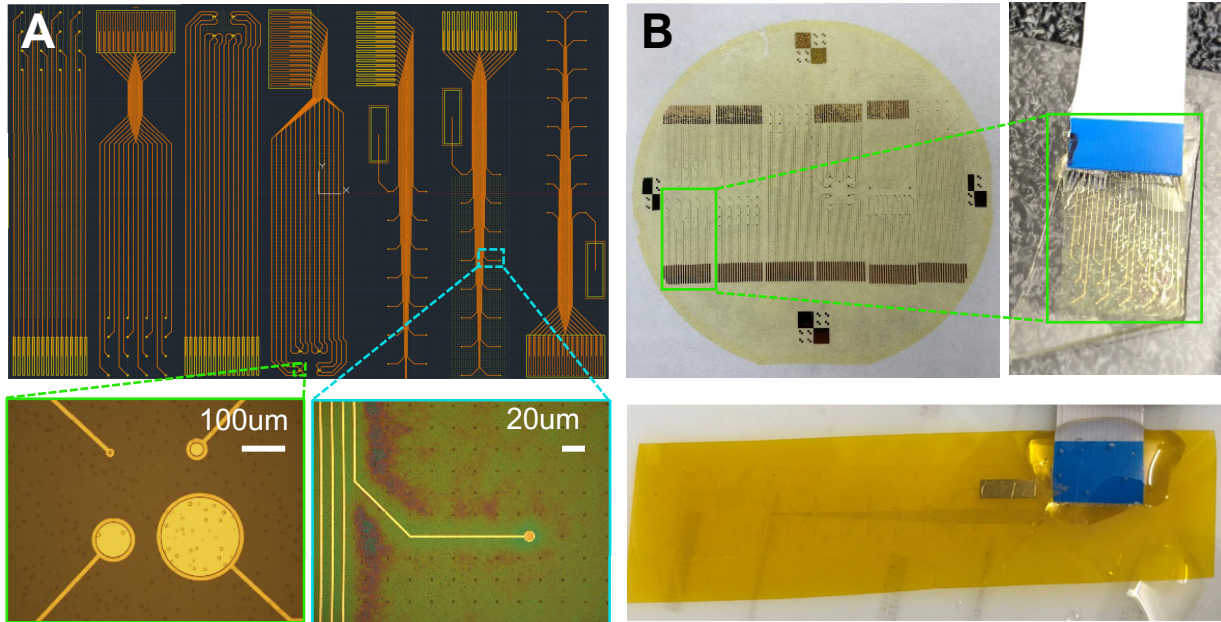


**Figure 2.2.1: Custom cleanroom fabricated flexible electrodes.** (A) Multi electrode arrays designed to conform to the mucosa surface, testing different structures for mechanical relief, electrode pitch, electrode size, and perforations to increase flexibility. (B) These electrodes were released from a three inch wafer onto water soluble tape, followed by transfer to Kapton tape or PLGA polymer and secured to an FFC connector with anisotropic conducting film and epoxy.

The fabricated electrodes were manufactured in the Harvard Center for Nanoscale Systems [a member of the National Nanotechnology Coordinated Infrastructure Network (NNCI)] on three inch silicon wafers (Nova Materials, CP02–11208-OX), in a protocol similar to [72]. The wafer was first cleaned with O2 plasma (100W, 2min, 50sccm), and a ~500nm layer of polyamide applied with a spin coater at 500rpm for 5 seconds followed by 3k rpm for 45 seconds. The wafer was then soft baked for 4 minutes at 65C followed by 2 hours at 200C, and cooled at approximately 5C/min to prevent cracking. This forms the bottom layer insulating layer to isolate the electrodes. Next, photoresist (LOR3A) was spin coated (500rpm for 5s, then 3k rpm for 45s) followed a soft bake for 3min at 115C and S1805 photoresist added in a similar fashion. The electrode designs were then exposed onto the wafer using a Heidelberg MLA150. After the wafer was descummed (O2 plasma at 30W, 30sec, 50sccm), 5nm of titanium followed

by 100nm of gold was deposited using an electron beam evaporator.  After deposition, the wafers were placed in acetone filled containers and placed on shakers for two hours for lift off, revealing the electrode designs.  To add the top insulating layer of polyamide such that the traces were not exposed to the environment, an additional layer of polyamide approximately 500nm thick was deposited as before.  To etch out the electrode pads, S1822 photoresist was spun onto the wafers (same settings), followed by soft bake at 115C for 5min, and then exposed using the maskless aligner as before after alignment. Finally, the windows were etched using the RIE8 followed by washing in CD-26 for four minutes to remove any remaining photoresist.  This resulted in approximately 1μm thick electrodes of multiple designs, with quality of windows and perforations shown in Figure 2.2.1A cutouts.

To release the electrodes from the wafer, water soluble transfer tape (SmartSolve, OH, USA) was placed on top of the wafer, the wafer was cracked from the other side, and the wafer was peeled away.  This left the electrodes stuck to the water soluble tape, with electrodes facing inwards (Figure 2.2.1B).  The electrodes were then released onto Kapton tape or a layer of Poly Lactic-co-Glycolic Acid (PLGA) polymer by carefully washing away the water soluble tape, leaving the electrodes outwardly facing and temporarily supported so as to not curl.  Following this, a 16 channel flat flexible cable was pressed onto the electrode pads with anisotropic conducting film (3M 7303) to provide a secure electrical connection.  Finally the interface was covered with epoxy to ensure a robust connection, with the end result shown in Figure 2.2.1B.

## 2.2.2 In-vivo measurements with Commercial Recording System

To determine a baseline of expected electrophysiology measurements from the stomach and evaluate these custom electrodes, an adapter board was made to connect the electrodes to a commercially available benchtop recording system.  The Open-Ephys (open-ephys.org) Acquisition Board with Intan (CA, USA) RHD2132 headstage connected to the electrodes via a FFC was used to record biopotentials at 30k samples per second with a resolution of 16 bits and a dynamic range of 15mV (Figure 2.2.3A).  This system was implemented during an in-vivo study in a sedated Yorkshire Pig, with all animal experiments approved by and performed in accordance with the Committee on Animal Care at MIT.  After sedation, access to the mucosa of the stomach was gained through laparotomy and the custom electrodes were removed from their Kapton support and placed directly on the mucosa (Figure 2.2.2B).
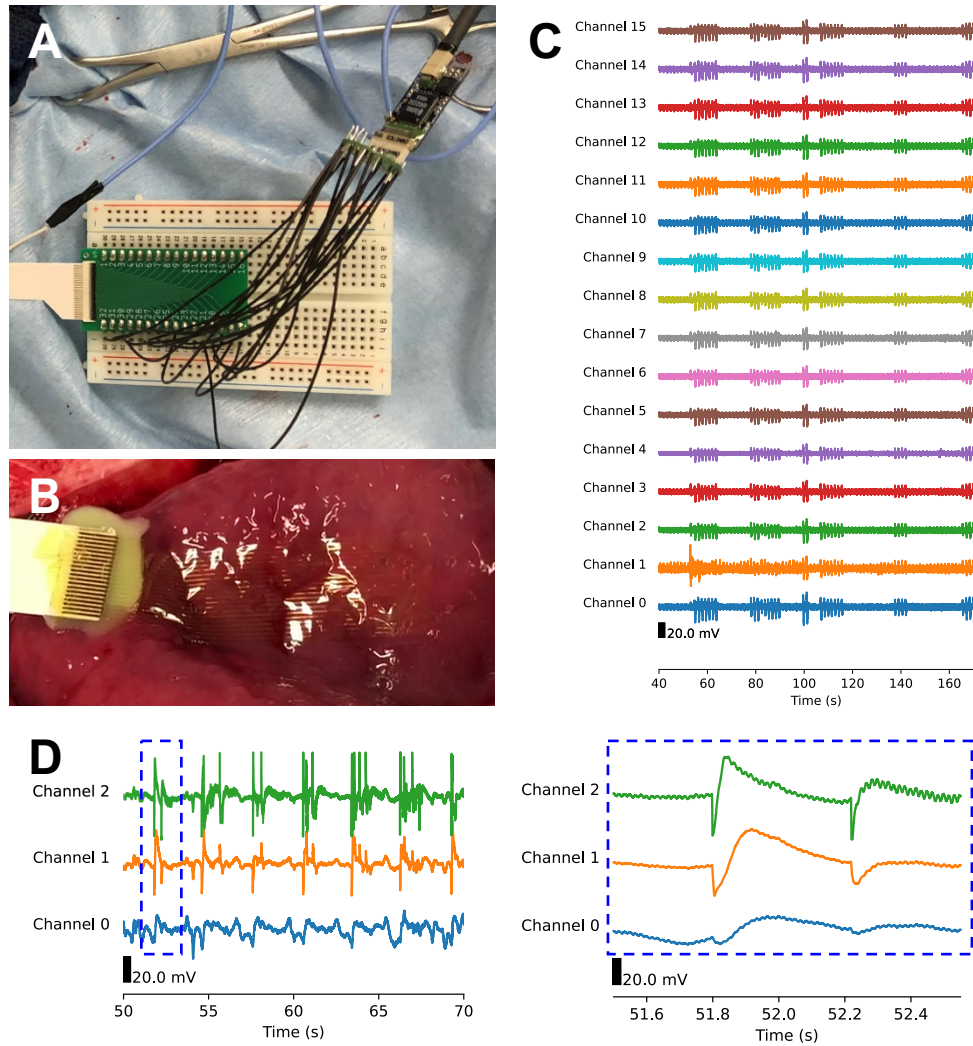
**Figure 2.2.2: Measurement results from commercial acquisition system.** (A) Connection from the FFC (attached to electrodes) to the Intan front end of the Open-Ephys system. (B) Custom electrodes conformed well to mucosa. (C) Data recorded on all channels for long periods of time. (D) Spike potentials observed.

The electrodes were seen to conform well, with contact verified by impedance measurements. With an AgCl electrode placed in at the bottom of the stomach, electrode impedances in the range of 0.18MOhm to 9.64MOhms were observed (a decrease of ~10MOhm compared to baseline). Recordings were seen in all channels with sets of spike potentials seen at a frequency of around three cycles per minute (Figure 2.2.2C), matching well with the expected frequency of the slow wave. However due to all the adapter boards adding parasitic capacitance combined with a high pass filter frequency of 1Hz (lowest possible setting), the slow wave

(around 0.05Hz) was not recorded.  Further evaluation of these electrodes is left as future work with MiGUT.

### 2.2.3 Flexible PCB Electrodes

To enable more rapid prototyping and a higher throughput of experiments, gold flexible electrodes were developed for the following experiments using commercial flexible printed circuit board manufacturing.  This has been shown to be successful in a number of previous experiments, e.g. [22], [28], [73], but with a focus on long term studies we wanted to record from multiple areas of the stomach instead of just one localized region.  As such, long flexible electrodes of 25cm in length that could conform to the greater curvature of the pigs' stomach were designed as shown in Figure 2.2.3A.  The low cost of these electrodes enabled us to obtain multiple designs, varying the electrode size and pitch for different applications.  Importantly, stiffener is applied to the connection end with a pitch of 0.5mm allowing for integration into the same FFC connectors as the previously designed electrodes.  Additionally, these electrodes can be easily rolled up on a 9mm roller and secured with water soluble tape for easy deployment into the stomach (Figure 2.2.3B).
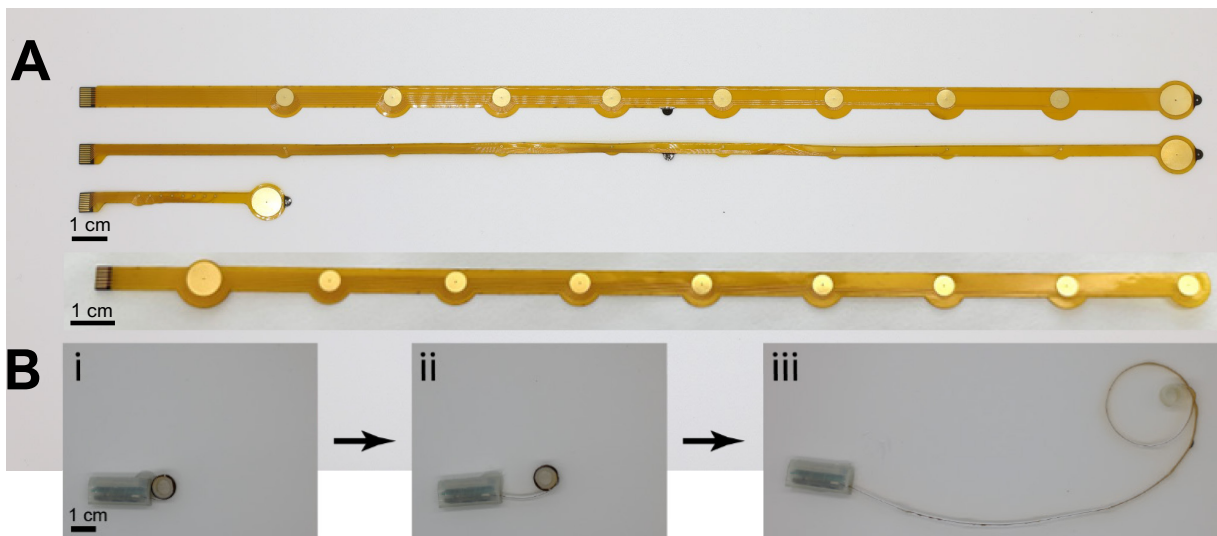


**Figure 2.2.3: PCB measurement electrodes.**  (A) Eight channel flexible electrodes with larger reference pad.  (B) Electrodes can be wrapped around a roller and deployed as a spring.

To ensure no cross talk between electrodes, two point impedance measurements were performed using a Sciospec ISX-3 Impedance Analyzer (Bennewitz, Germany).  Figure 2.2.4

shows high impedance between two adjacent electrodes and a high impedance between each electrode and the reference electrode. This suggests there is enough isolation between each channel to ensure independent measurements.
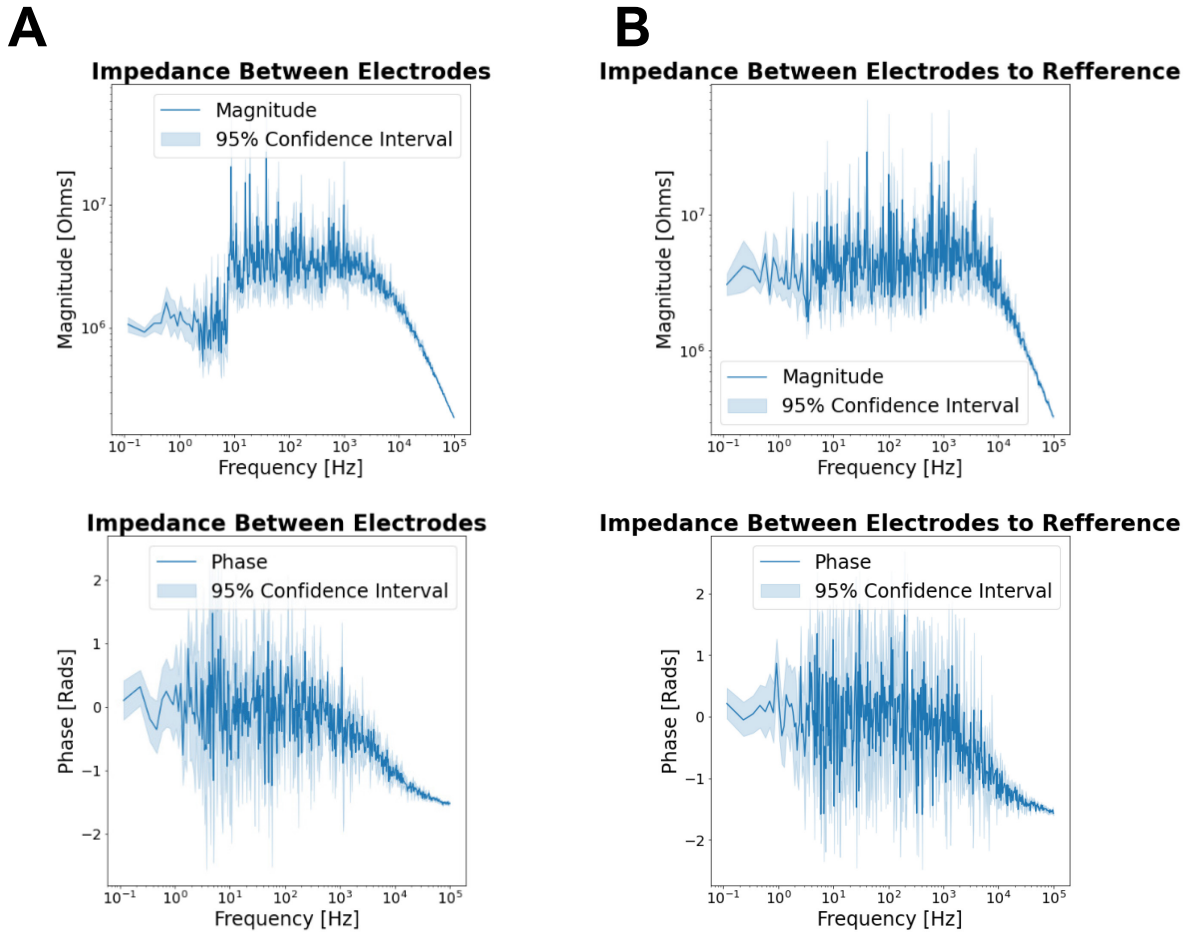


**Figure 2.2.4: PCB electrode impedance.** (A) Impedance between two adjacent channels. (B) Impedance between a channel and the reference electrode.

While not tested using the benchtop system, motivated by the success of previous work we successfully implemented these electrodes with MiGUT to achieve high quality results in-vivo.

## 2.3 Low Power, Wireless Electronics

### 2.3.1 Initial Prototype

First, an initial prototype was developed to show all the necessary components could be integrated into a custom printed circuit board in an ingestible formfactor. A six layer PCB was designed to sample data at 215 samples per second per channel using a 16bit four channel analog to digital converter (ADC; Texas Instruments ASD1115), send the data to a microcontroller for data handling (Analog Devices ADuCM355), and wirelessly transmit the data using a 915MHz transceiver (Semtech SX1231). This system, enabled by the ADuCM335, could also perform impedance measurements and cyclic voltammetry to test other ingestible sensors. All of this was integrated into a 25x10mm$^2$ PCB shown in Figure 2.3.1, which could be powered by size 13 hearing aid coin cell batteries (Duracell). However the current draw of the device peaked at 112mW during transmission significantly reducing the battery life, even when heavily duty cycled. While only four channels were bipolar on the dedicated ADC, eight additional ADC inputs along with the two chemical sensing channels were made available from the microcontroller with an additional flat flexible connector. Thus, we successfully showed all necessary components could be further miniaturized from the current state of the art ingestible devices (compared in section 2.3.6), a key step to enable clinical translation of this system.
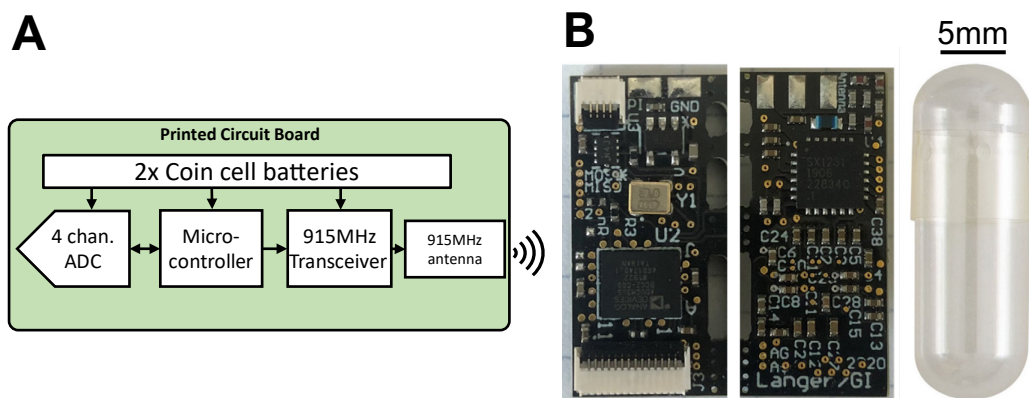


**Figure 2.3.1: Initial electronics prototype.** (A) Overall schematic. (B) Top and bottom of designed PCB with comparison to 000 sized capsule.

## 2.3.2 MiGUT Overview

After developing the first iteration, the final device was designed to improve the size, battery life, and ease of assembly. MiGUT is shown in Figure 2.3.2A which consists of an electronics module with a daughter board providing power, and can connect to a number of flexible measurement electrodes via a flat flexible connector. The electronics are housed in a $9x12x26mm^3$ 3D printed case (Figure 2.3.2B) which was designed to be comparable to DFA cleared products such as the capsule endoscopy systems (Medtronic PillCam, $\varnothing11x26mm^3$ [57]) to facilitate future clinical translation.
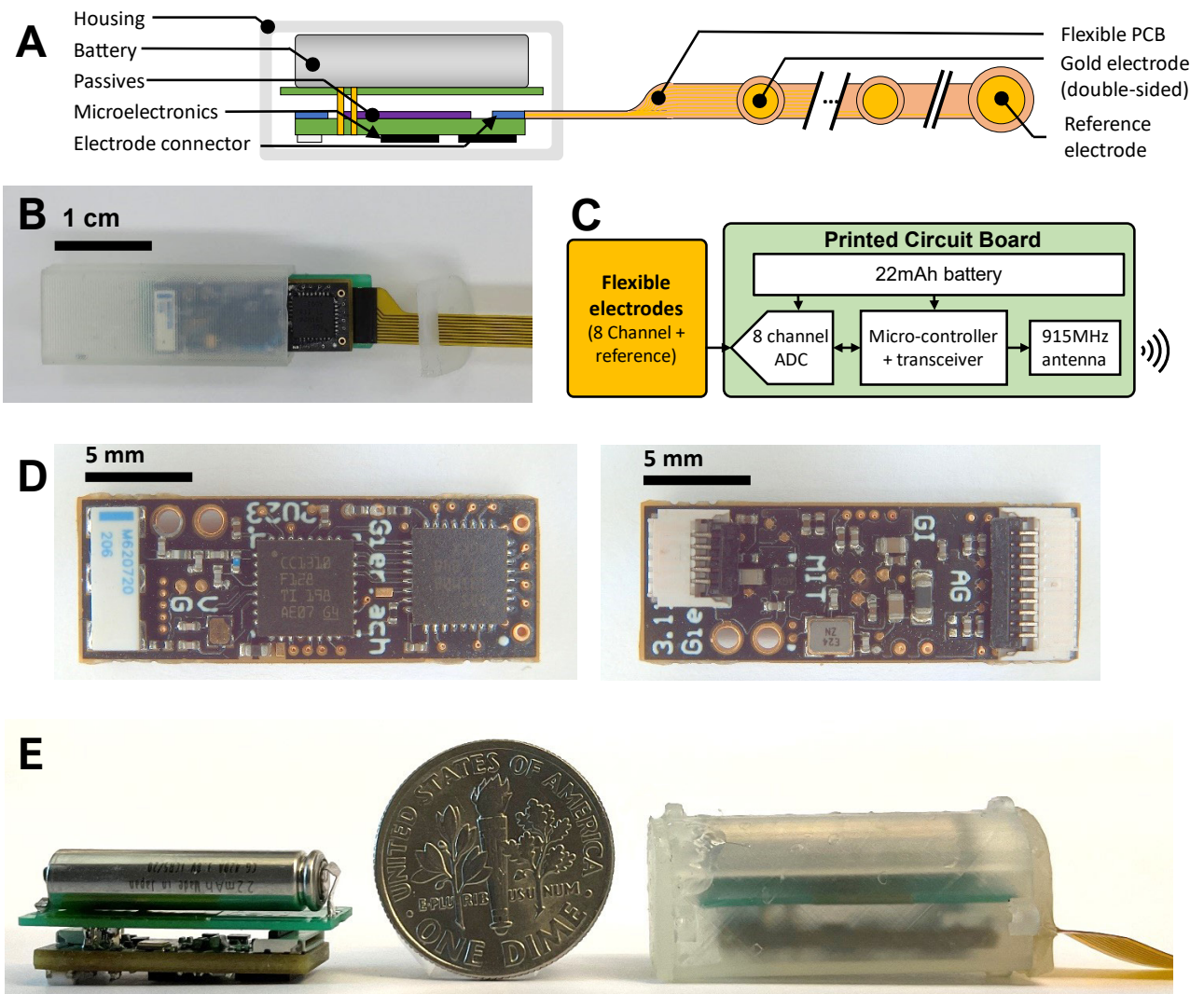


**Figure 2.3.2: MiGUT Overview.** (A) Overview of key components. (B) Device assembly. (C) Device schematic. (D) Device electronics. (E) Assembled device.

With a focus on miniaturizing MiGUT even further compared to the initial prototype, the Texas Instruments CC1310 microcontroller with integrated transceiver was selected to control the sensing peripherals and handle wireless communication. We used the 4x4mm$^2$ package for the CC1310 which is smaller than the initial versions microcontroller alone, at the cost of the TIA, impedance measurements, and digital waveform generators present in the ADuCM355 – valuable for other experiments but not critical for the design. This enabled the incorporation of the Texas Instruments ADS131M08, a more versatile eight channel 24bit simultaneous ADC. This ADC was selected for its ability to record bipolar potentials simultaneously at configurable data rates from 65.4 samples per second to 8k samples per second (in very low power mode). All channels share the same reference, which are connected to the reference pin of the FFC header. For efficient data movement and wireless communication, the ADC was set to digitize with 16bits. The updated schematic is shown in Figure 2.3.2C, with the detailed schematic containing passives and power circuitry in Appendix A.

This schematic was realized on a six layer custom printed circuit board measuring 7x19.6mm$^2$ (Figure 2.3.2D) manufactured using 1.6mm FR4 substrate, 1Oz copper traces, and ENIG pad finishes. The Flat Flexible Connectors (FFC; Molex 5034801000), Analog-to-Digital Converter (ADC; Texas Instruments ADS131M08), microcontroller with integrated transceiver (Texas Instruments CC1310), crystals (ECS ECS-240-6-37B2-JTN-TR and Abracon ABS04W-32.768KHZ-6-B2-T5), and power regulator (Onsemi NCP170AMX330TBG) were then assembled with leadless solder. To power the device, a two layer daughterboard measuring 7.16x22.46x0.51mm$^3$ was used to securely mount the 22mAh Panasonic CG-420A Li-ion battery and is connected to the six layer PCB with headers that are soldered in place (Figure 2.3.2e left). This enables different power configurations to be used in the future depending on the study requirements. A Li-ion battery was chosen to support the continuous high current draw during wireless streaming of data, with more details in section 2.3.3. The 915MHz antenna (Ethertronics/AVX M620720) was positioned on the outside face of the device to maximize radiation efficiency with recommended keep out regions, a pi matching network was implemented with datasheet recommended values, and large group planes used. Impedance analysis using a Vector Network Analyzer (Keysight E5080B) showed the antenna was not matched, but still showed acceptable performance in-vivo as discussed in section 2.3.4.

The device was then placed in a 3D printed case (Figure 2.3.2E right) fabricated using a Formlabs 2 3D printer (Durable Resin), with end caps press fit together, and sealed with UV cure epoxy (Loctite 4305), bringing the final dimensions to 9x12x26mm$^3$. (This could be made smaller with higher tolerances on the case). The electrode ribbon is connected to the FFC connector before placing into the case, with the electrodes fed through a slot in one of the end caps, and then sealed with the UV epoxy. For experiments where a roller was used, the electrode ribbon was bound to a 9mm diameter roller using water soluble tape as shown in section 2.2.4 for ingestible delivery with automatic deployment once the device reaches the stomach. For experiments where endoscopic clipping was used, nylon loops can be passed through mounting points in the 3D printed case at the front and back ends of the capsule. Additionally, a nitinol loop can be passed through the via located on the double-sided reference electrode for secure placement of the flexible electrodes and ensuring a secure interface with tissue.

Further reductions in size could be achieved by using tighter PCB manufacturing tolerances, different battery configurations, or combining all the components into a single custom integrated circuit. Other deployment and retention mechanisms can easily be integrated into the case for ease of deployment and retention.

## 2.3.3 Software Flow and Power Management

The current consumption of the device depends on the sampling frequency of the ADC, frequency of wireless communication, and duty cycling rate – all of which can be programmed ahead providing flexibility in balancing experiment length and signal fidelity. First, the Cortex-M3 microcontroller is programmed to initialize the ADC for low power and 16bit resolution mode, at a specified sampling rate and signal amplifier gain configuration. For the in-vivo experiments presented, a sampling rate of 62.5 samples per second was selected for power efficiency and a range of ±600mV or ±150mV was selected depending on the length of experiment to account for baseline drift. Then, the device transmits a confirmation it was successfully initialized and then transitions to an ultra low power mode for a programmed amount of time. Two programmable arrays allow for complete customizability in the duty cycle ratio over multiple recording events. Unless otherwise specified, for ambulation experiments the device is turned on immediately before placement (to allow for confirmation of functionality once assembled), sleeps for two hours, then records 168750 samples (for 45 minutes, to capture

long trends), and sleeps for 22 hours (a 2% duty cycle ratio). During sampling, the ADC triggers an interrupt when new data is ready, which is then loaded into a buffer that transmits the data immediately in parallel to receiving new data. While schemes for saving the data were explored, streaming the data was found to be more robust in ambulating experiments to ensure minimal interruption of data if one of the packets was corrupted. For low sampling rates, the device is automatically able to go into a lower power state after transmission while it is waiting for the next sample. The data is then wirelessly transmitted as described in section 2.3.4.

To evaluate the trade-off between data throughput and power consumption, the current consumption of the device was measured using the Nordic Semiconductor Power Profiler Kit II under different device configurations. These measurements were validated in long term current consumption measurements using a Keysight 34465A digital multi meter. When configured to sample at 62.5 samples per second and stream the data continuously, MiGUT consumed an average of 6.64mA with peaks at 16.88mA. During sleep mode MiGUT consumed 6uA on average. The results when changing the sampling rate are shown in Figure 2.3.3A.
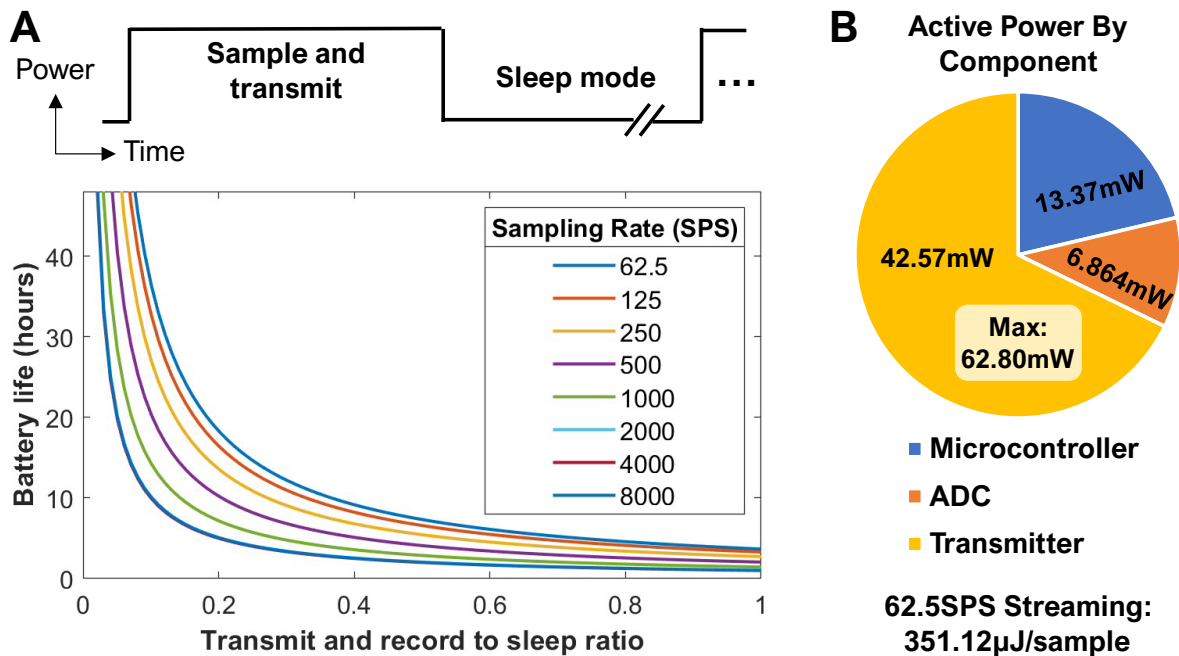


**Figure 2.3.3: MiGUT battery life.** (A) Depending on the selected sampling rate and duty cycling ratio, the device can provide high quality recordings ranging from a few hours to days depending on the needs of the experiment. (B) Wireless transmission consumes the most power, followed by microcontroller data handling and clock generation, and then ADC power consumption.

While a Li-ion battery was chosen to ensure the high current peaks during wireless transmission would not damage the battery (Figure 2.3.3B) and allow for more efficient use via recharging, silver oxide batteries are more commonly used in ingestible devices for their safety [65]. Thus, in addition to the Panasonic CG-420 li-ion, two Murata SR626 (1.5V 28mAh) and two Renata 393 (1.5V 80mAh) in series were separately tested to show compatibility for future translation. While the two Murata SR626 configuration only lasted approximately five minutes before continually resetting and unable to maintain nominal operation, the two Renata 393 battery configuration was able to last 7 days. This is 3.5x times longer than the Panasonic CG-420, with only a slight size increase of 1.5x, at the cost of being unable to recharge and a cylindrical form factor. In cases where the smaller form factor of the Murata SR626 battery is more desirable, the transmit power of the device can be lowered. Figure 2.3.4 shows the current consumption of only the CC1310 during different transmit power levels. This can be correlated with the datasheet or other stress tests to choose a transmit power level with acceptable current peaks for each battery, such as 9dBm for the Murata SR626.
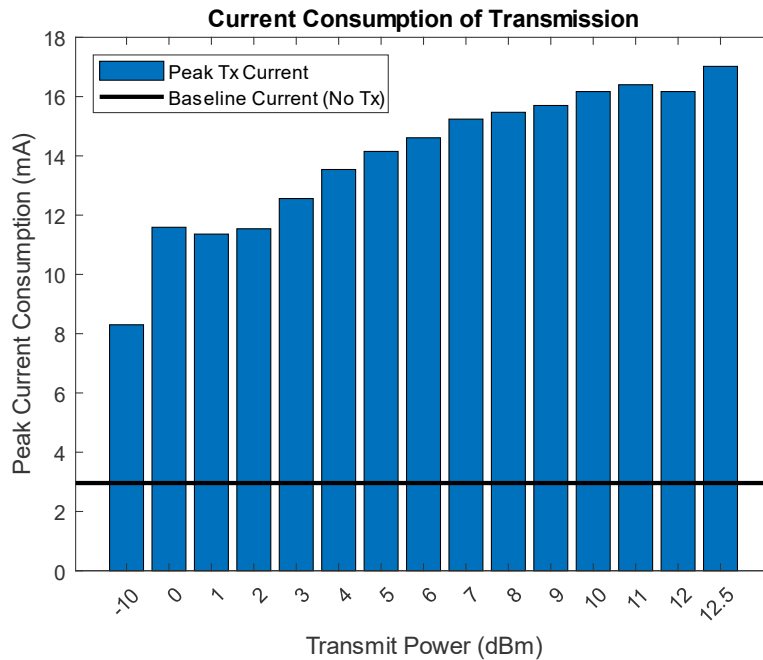


**Figure 2.3.4: MiGUT current consumption at various transmit power levels.** A packet of length 18 bytes was transmitted with all other components shut down. The baseline current consumption of the microcontroller can be seen as approximately 3mA, with higher transmit powers requiring higher current.

## 2.3.4 Wireless Communication

Data from MiGUT is wirelessly transmitted at 12.5dBm transmit power using a 500kBps symbol rate at 915MHz with a deviation of 175kHz and receiver filter bandwidth of 1242kHz. Data from all channels are transmitted with a packet number and checksum CRC for error correction as they arrive from the ADC, resulting in a packet of 20 bytes plus address and preamble. Generally, shorter packets were found to be received more effectively, with longer packets generating more likely to be corrupted during transmission in non-ideal conditions, though this was not thoroughly explored. The 915MHz communication frequency was chosen for its greater penetration depth and proven track record in ingestible devices [56], [66].

Tests with Bluetooth Low Energy were also performed contributing to [74] and showed extra considerations are required when trying to implement Bluetooth communication in an ingestible formfactor. Figure 2.3.5 shows the impact of different spacing between an antenna and the case when placed in a 500mL beaker of water. While this shows the absolute signal strength can be made acceptable, the bit error rate of the signal was found to cause issues when attempting to connect during in-vivo studies. A benefit of 915MHz is that the packets are consistently transmitted at one frequency (compared to frequency hopping possibly during Bluetooth connections) and does not require a handshake to start communication.



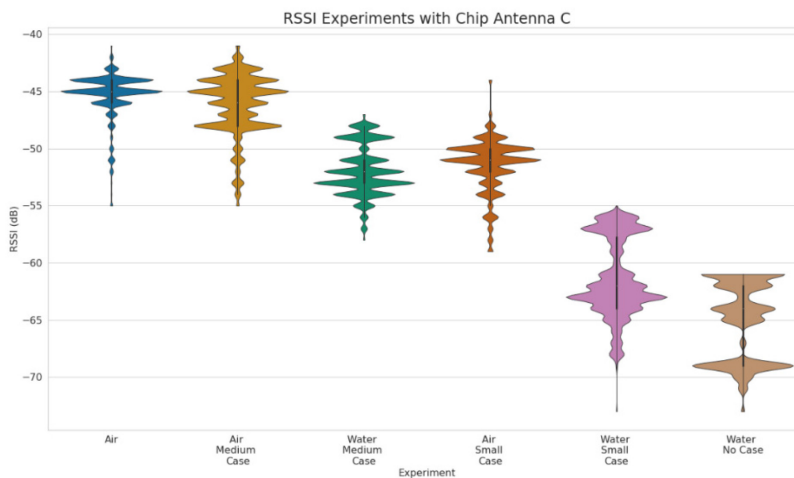**Figure 2.3.5: Signal strength of BLE chip antenna in water.** The Received Signal Strength Indicator (RSSI) when a chip antenna is placed in 500ml beaker filled with water, 30cm away from the receiver, in air, a case with medium air gap, and small air gap. The medium case does not significantly impact performance in air and causes less of a performance drop when placed in water compared to the small case in and out of water.

A Texas Instruments LAUNCHXL-CC1310 evaluation board with panel antenna (TE Connectivity PAL902010-FNF) was connected to a laptop and used with Texas Instruments SmartRF Studio 7 (version 2.23.0) to save the received data to a text file. While a benchtop receiver setup was used, commercially available USB dongles such as the Texas Instruments CC1111EMK868-915 can enable data to be recorded to a mobile device. With the panel antenna approximately one to four meters away from the device in a freely moving Yorkshire pig (97kg), an external 915MHz transceiver was found to reliably receive over 99% of data from MiGUT at approximately -70dBm in a full stomach and during multiple behaviors (Figure 2.3.5).
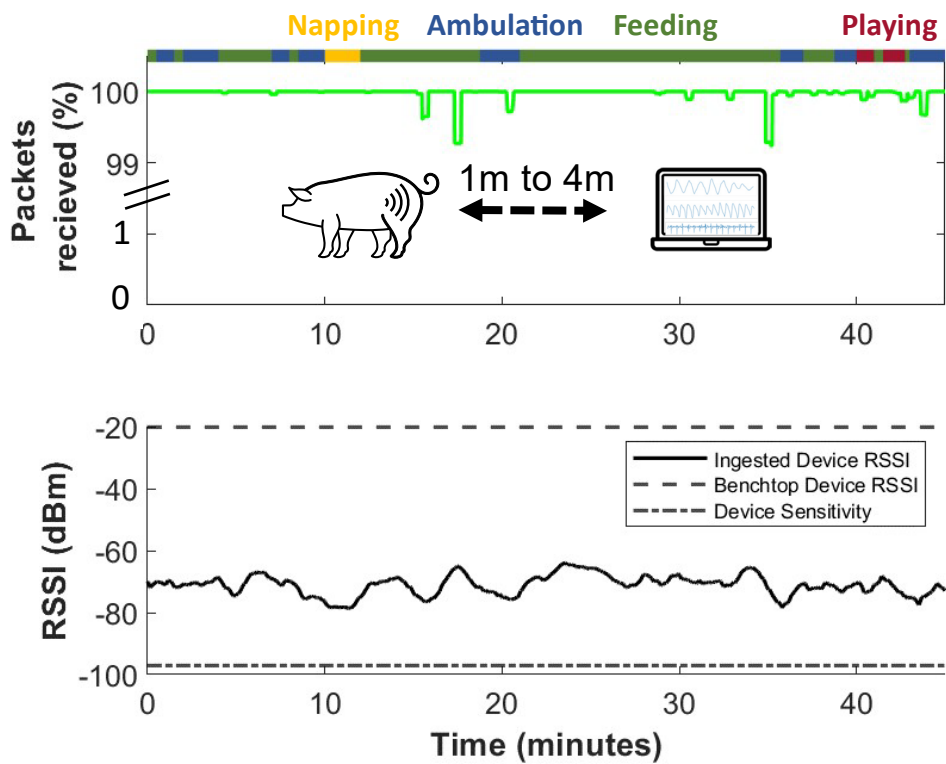


**Figure 2.3.5: Wireless performance of MiGUT.** Excellent communication is maintained with minimal data loss from the device in an ambulating animal during multiple behaviors. The Received Signal Strength Indicator (RSSI) was always well above the sensitivity of the device.

To determine the minimum transmit power required for effective communication, the packets were repeated and transmitted at different transmit power levels in a different 87kg pig. The results shown in Figure 2.3.6 show that good communication can be maintained from +12.3dBm to approximately 4dBm, after which the RSSI drops and the bit error rate increases considerably. Due to the structure of the enclosure, which contains metal walls that could

impede wireless signals, we continue to use +12.5dBm to ensure an adequate safety margin. However in less obstructed environments, if +4dBm transmit power is acceptable this would correspond to a 1.8x power decrease (see Figure 2.3.4).
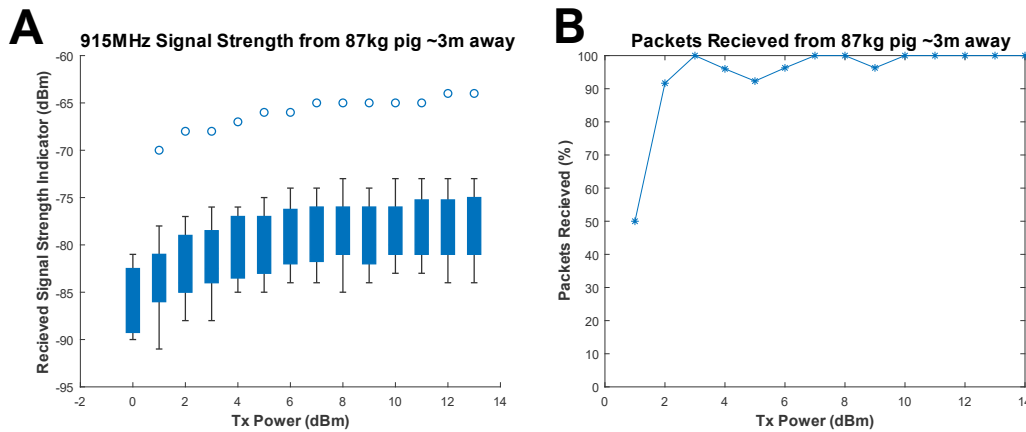


**Figure 2.3.6: Communication in-vivo at different power levels.** (A) Received Signal Strength Indicator and (B) packets received sweeping all transmit power levels. No packets were received transmitting at -10dBm.

## 2.3.5 Measurement Validation

To validate the operation of each device, a known stimulus is injected into the electrodes in addition to power profile measurements. A 1Hz 200mV peak to peak square wave generated by a signal generator (Keysight 3000T with DSOX3WAVEGEN or Rigol DS1104Z-S Plus) was measured on all channels individually to confirm sampling rate and correct voltage decoding. Other signals were also tested over a variety of amplitudes and frequencies, and the correct output was seen to be received with no cross talk. One such test is shown in Figure 2.3.7.

**Wirelessly Transmitted Signals**
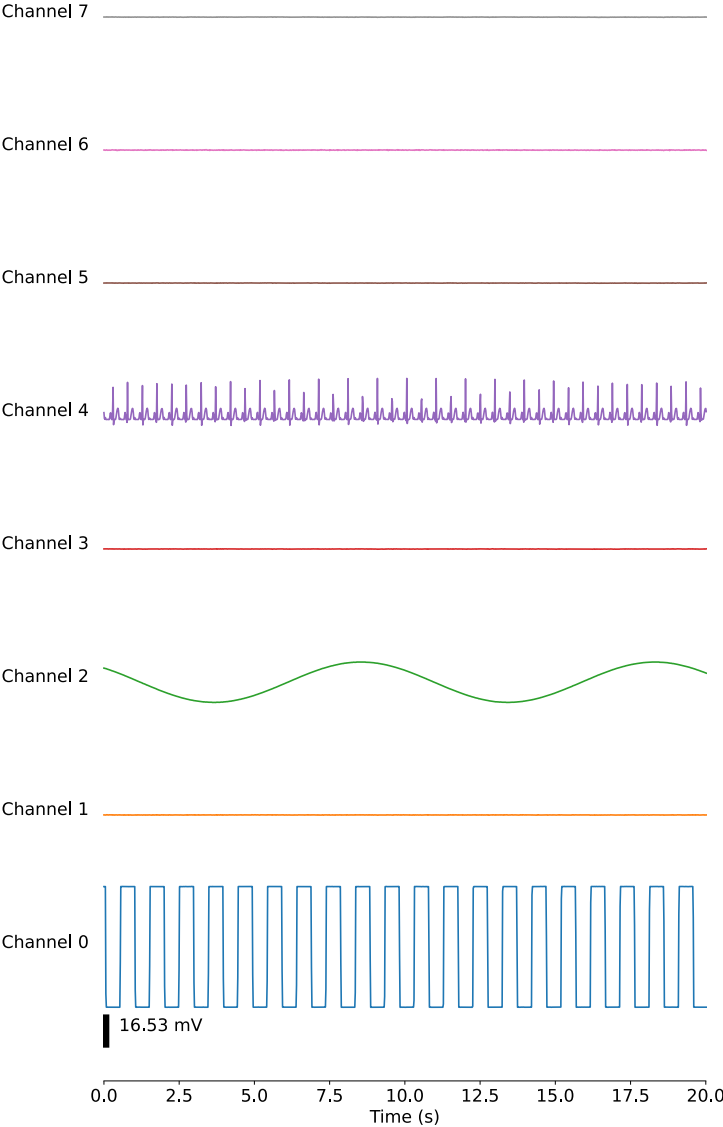


**Figure 2.3.7: Received wireless test signals.**  A 60mVpp 1Hz square wave was injected into channel 0, a 20mVpp 100mHz sine wave on channel 2, and a 40mVpp 2Hz cardiac signal on channel 4 was correctly received.

## 2.3.6 Comparison to State of the Art

A comparison of MiGUT is presented in Table 2.3.1.  In comparing MiGUT with the state of the art, it is currently the smallest multi channel ingestible.  As previously discussed, this is very significant for clinical translation to ensure it will not cause a blockage while also

allowing for endoscopic placement enabling easy placement of the device for long term studies without the need for laparotomy. While an application specific integrated circuit was developed by Ibrahum et al, it has yet to be implemented in-vivo. Of special note is that MiGUT currently has the highest sampling rate of available devices, enabling measurement of spiking action potentials in addition to tracking the slow wave.

**Table 2.3.1: Comparison to state of the art.**

| Paper | Wang et al. [41] | Paskaranandavadivel et al. [42] | Javan-Khoshkholgh et al. [43] | Ibrahim et al. [44] | **MiGUT** |
|---|---|---|---|---|---|
| Size with Battery ($mm^3$) | 3346 | 8680 | 4840 | $25mm^2$ ASIC | **2552** |
| Recording Channels (#) | 3 | 7 | 32*2 (MUX) | 64 | **8 (indep.)** |
| Sampling Rate/Chan (SPS) | 90 | 100 | 15 | 244 | **62.5 (up to 8k)** |
| Resolution (bits) | 12 | 8 | 12 | 10 | **16 (24 available)** |
| Communication Frequency | 433MHz | 2.4GHz | 2.4GHz + 13.56MHz | 13.56MHz | **915MHz** |
| Placement | Implanted in greater curvature | Intestinal serosa | Benchtop | Benchtop | **Stomach mucosa** |

# Chapter 3 In-Vivo Validation of MiGUT in Anesthetized Animals

In-vivo demonstration of MiGUT was first performed under controlled conditions to ensure adequate signal acquisition, in addition to the performance characterization already shown. While some early experiments with the initial prototype and cleanroom electrodes were performed in a terminal setting with surgical access via laparotomy, all experiments shown below were done with endoscopic placement.

## 3.1 Device Placement Under Anesthesia

All animal experiments were approved by and performed in accordance with the Committee on Animal Care at MIT. Yorkshire swine were obtained from Cummings School of Veterinary Medicine at Tufts University (Grafton, MA, USA) for in-vivo experiments. Pigs weighing approximately 60-100 kg were placed on a liquid diet for 24 hours the day before the study and were fasted overnight prior to the study. For device placement, animals were anesthetized using an intramuscular injection of midazolam 0.25 mg/kg and dexmedetomidine 0.03 mg/kg. Following sedation, animals were placed on thermal support and ophthalmic ointment was applied to both eyes. The animal was intubated and placed on isoflurane (2%) in oxygen and connected to a vital signs monitoring system. MiGUT was delivered orally into the stomach, using an orogastric tube and imaged using PENTAX EC-3870TLK (160 cm) to visualize the stomach with the animal in the left lateral position.

During these studies, two formfactors were tested. Initially, the device was placed with electrodes trailing the capsule as shown in Figure 3.1.1A. To ensure no stress was placed on the capsule-electrode interface, a particularly brittle area after sealed with the epoxy, the device is pulled down the endoscope using the gripper. This ensured the electrodes were not damaged during delivery. Later, to showcase this could be taken orally without endoscopy, the roller configuration described in 2.2.4 was used. This allowed the device to be pushed on the other side while protecting the electrode interface.
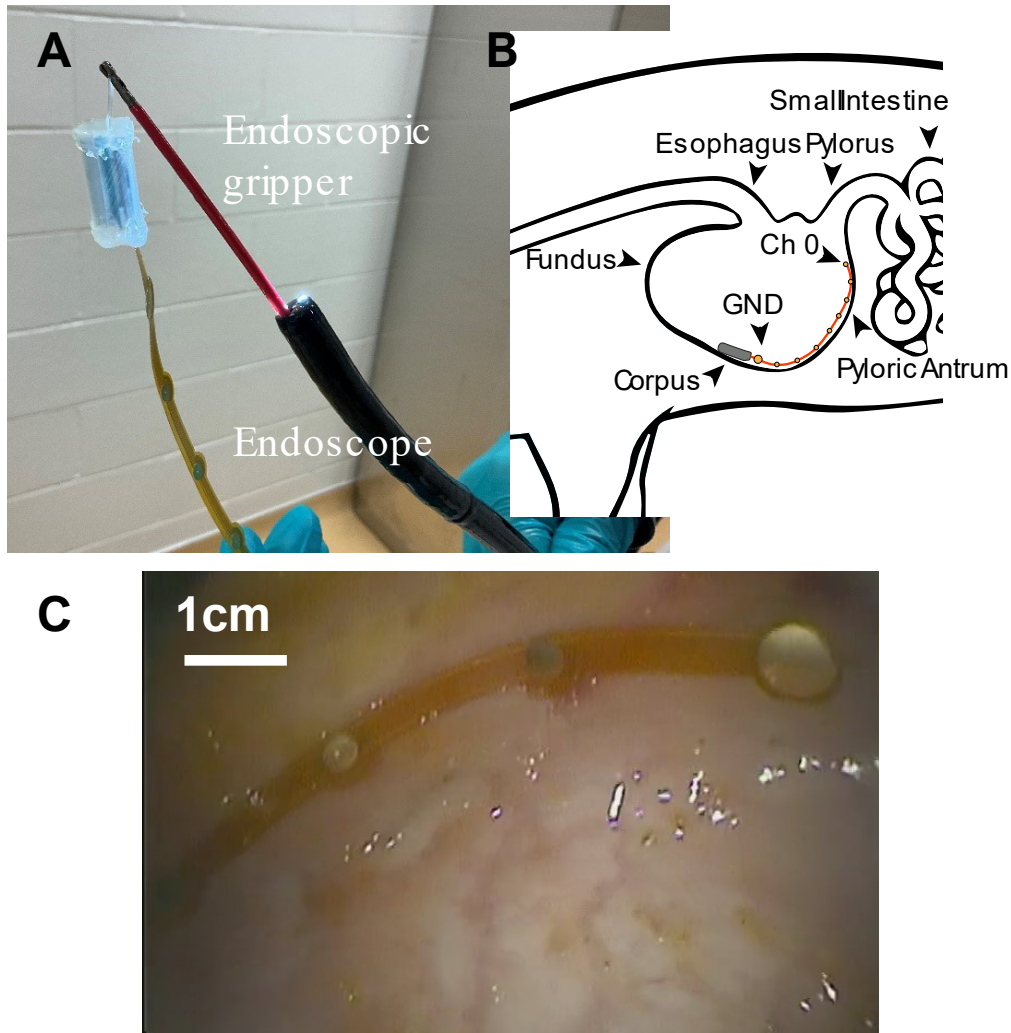
**Figure 3.1.1: Placement of MiGUT in-vivo.** (A) To safely place the device, the MiGUT device was pulled down the over tube using the endoscopic gripper, ahead of the endoscope. (B) The electrodes were localized from the corpus to the pyloric antrum along the greater curvature of the stomach, shown in-vivo in (C).

Nine experiments were performed under anesthesia, the data from which is shown below. In these experiments, the electrodes were positioned such that the reference electrode was localized near the stomach corpus as shown in Figure 3.1.1B. These experiments lasted on average 1.5 hours.

## 3.2 Data Processing

Biopotentials were recorded at 62.5 samples per second, with a representative sample shown in Figure 3.2.1A. It is encouraging that a signal with similar to the slow wave can be easily picked out from most channels. Immediately following device placement (t=0 to 500

seconds), electrical activity is seen in all channels likely as a result of mechanical stimulation because of endoscopic visualization following device deployment (Figure 3.2.1B). As such, only recordings approximately 10min after the endoscope was removed considered with early noisy data being truncated. To isolate the multiple types of periodic waveforms observed, bandpass filtering using a third order Butterworth filter was used. In these experiments with the reference closest to channel zero, we see there is less of a change for channels closer to the reference. Of the nine studies, one dataset was omitted due to a simultaneous study resulting in high levels of noise.



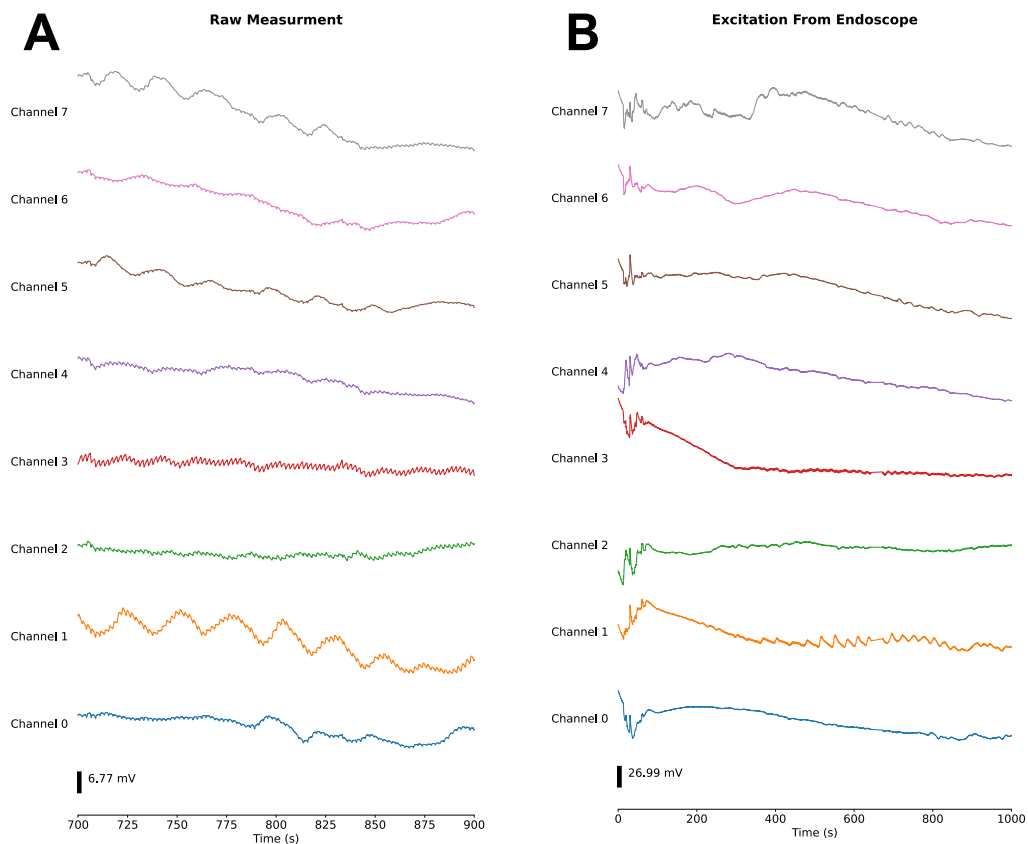**Figure 3.2.1: Raw measurements from an in-vivo study.** (A) The slow wave can be seen in measurements without any filtering. (B) Abnormal activity immediately following device placement.

## 3.3 Multimodal Signal Analysis

Three signals were seen to be superimposed on the raw signal shown in Figure 3.2.1. When filtering in the frequency of the slow wave, a continuous periodic waveform with mean

amplitude of ~5mV and frequency approximately 3cpm is seen (Figure 3.3.1A).  Similarly, filtering at a slightly higher frequency shows a periodic waveform with mean amplitude of ~1mV at a frequency of 26cpm (Figure 3.3.1B).  Finally, at a frequency of 90cpm a spiking waveform can be seen with mean amplitude of ~0.05mV (Figure 3.3.1C).  These components of high spectral energy correspond well with the recorded heart rate and respiratory rate monitored during the study.  This supports that MiGUT can be used not just for tracking gastric slow waves, but also other vital signals which can be tracked individually or as an input to on-device algorithms.
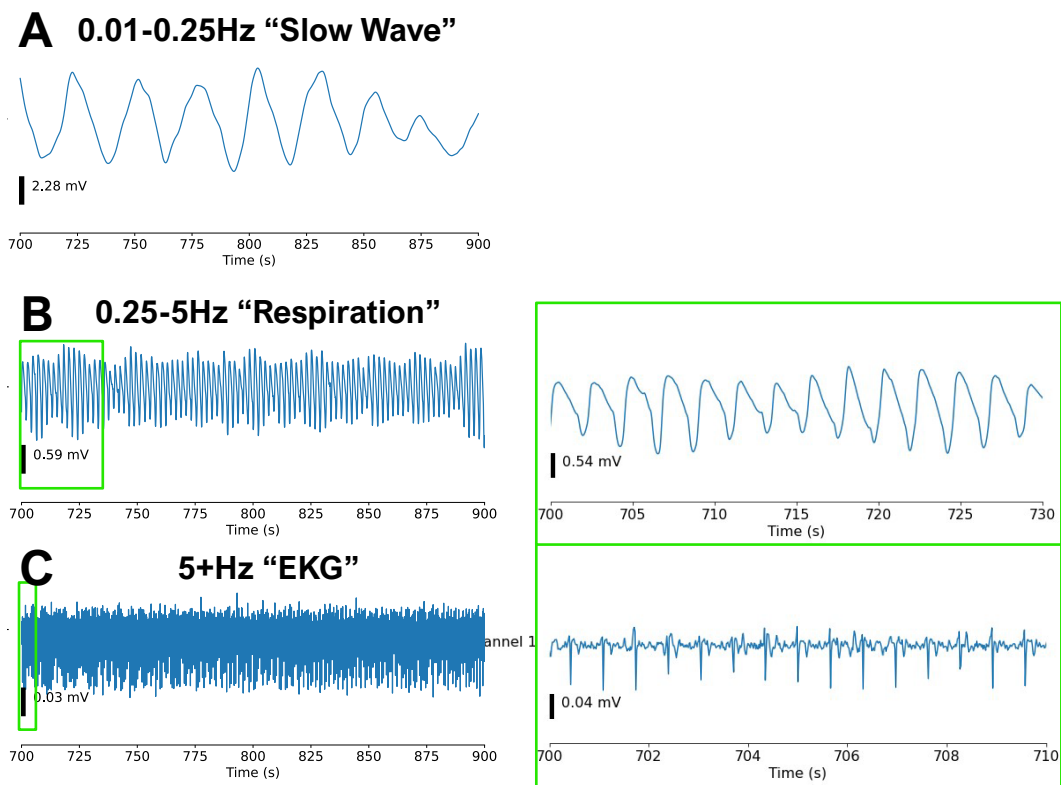


**Figure 3.3.1: Multimodal measurements.**  Filtering to the respective bands reveals (A) the slow wave, (B) respiration, and (C) heart rate.

In addition to the data presented in Figure 3.2.1, an even slower periodic signal can be seen highlighted in Figure 3.3.2.  Large amplitude waveforms were observed for six cycles with a period of approximately 500 seconds near the pylorus (chan. 0-2).  This has not been previously reported in literature, possibly due to signal processing schemes focused on the expected slow wave frequency range.  These signals may be attributed to the Migrating Motor Complex (MMC), which occurs on timescales from 90 to 120 minutes [75]. More investigation

is required, but these signals possibly point to additional control related activity either related to the MMC or as an intermediary process.
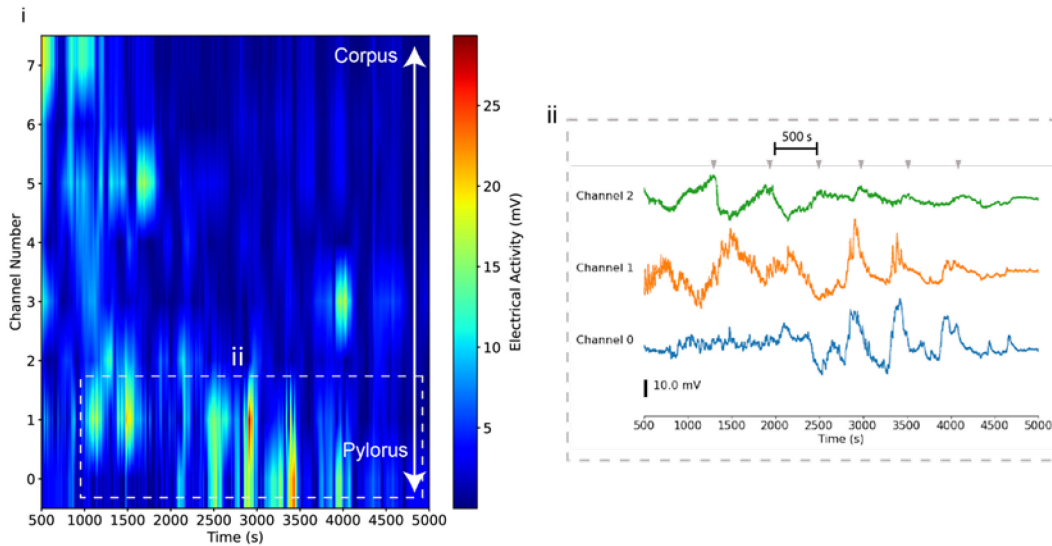


**Figure 3.3.2: Ultra long periodic signals recorded.** Over 1.5h of recording (i) heatmap after bandpass filtering from 0.005 to 15 Hz and (ii) punch in on channels near the pylorus showing periodic signal with an approx. 500 second period.

To ensure these signals are indeed of biological origin, in one study a barbiturate cocktail [Fatal Plus (sodium pentobarbital), 1ml/10lbs] was administered during a recording session. As seen in Figure 3.3.3, after administering the cocktail the slow wave (and all other signals) terminated. This indicates that these signals were not due to noise in the environment or the recording setup.



**Figure 3.3.3: Cessation of electrical signals.** A barbiturate cocktail administered at t=125s stops the slow wave from being observed.

## 3.4 Prokinetic Study

Finally, to show this system can track changes in motility, Azithromycin was administered halfway during six studies. Azithromycin is a prokinetic that has been shown to

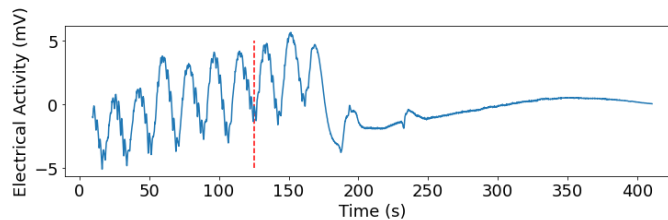increase motilin receptors [76]. It was intravenously delivered at 1mg/kg over 5 minutes through an ear catheter. After administration, a significant increase in the amplitude of the slow wave was observed in five of the recording channels shown in Figure 3.4.1A. However, no significant changes were seen in the respiration and heart rate frequency bands, with the EKG signal still clearly seen (Figure 3.4.1B). This indicates throughout this duration of increased gastric activity (with suspected contractions [76]), the electrodes continued to make good contact. Thus, we show MiGUT is able to track changes in gastric motility and maintain a reliable interface with the mucosa.
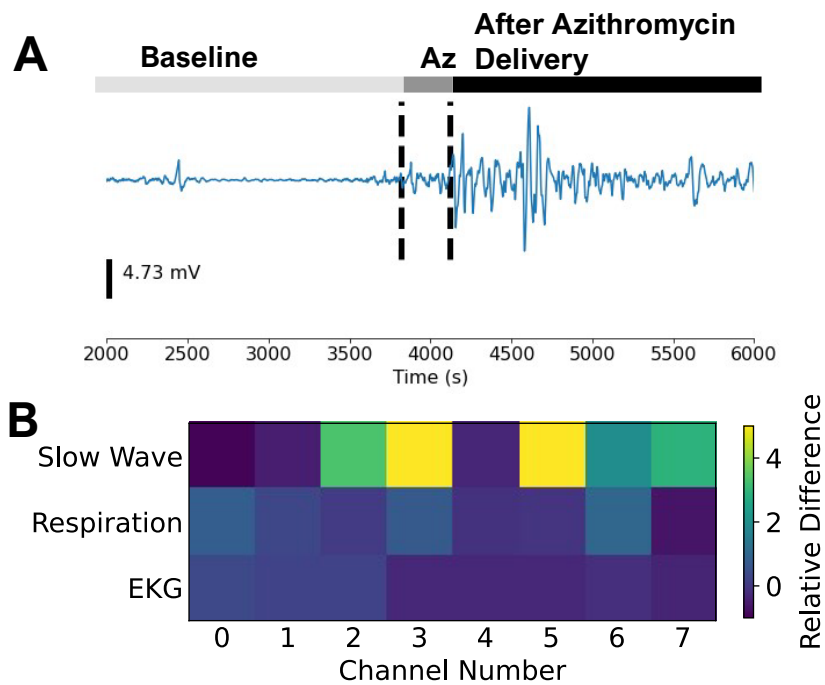


**Figure 3.3.4: Impact of prokinetic on recorded activity.** (A) Slow wave activity (0.01-0.25Hz bandpass filter) before and after administration of azithromycin. (B) Relative difference in signal power before and after administration for different frequency ranges.

# Chapter 4 In-Vivo Demonstration of MiGUT in an Ambulating Animal

After MiGUT was shown to reliably track multiple biopotentials in the stomach and maintain a quality connection with the mucosa, we wanted to capture data from an ambulating large animal – something that has not been reported in an ingestible form factor.

## 4.1 Placement with Retention

To ensure the device would not pass through the pylorus and have a better reference (with low electrical activity) over long recordings, the device was localized such that the reference was near the fundus with the electrodes running along the greater curvature of the stomach as shown in Figure 4.1.1A. Placement of the device mirrored what is described in section 3.1 with the exception that after delivery to the stomach, three endoclips (Boston Scientific Resolution Clips) were used to secure the device to the mucosa. These Resolution clips have been shown in literature to stay fixed for a few weeks [77], [78], however much stronger endoclips such as the Ovesco clip could be used for longer residency up to 24 months [79]. Two clips were used to secure the capsule on either side using nylon thread (Figure 4.1.1B), and an additional clip was used to secure the reference electrode by a nitinol wire loop through a hole on the reference electrode (Figure 4.1.1C).
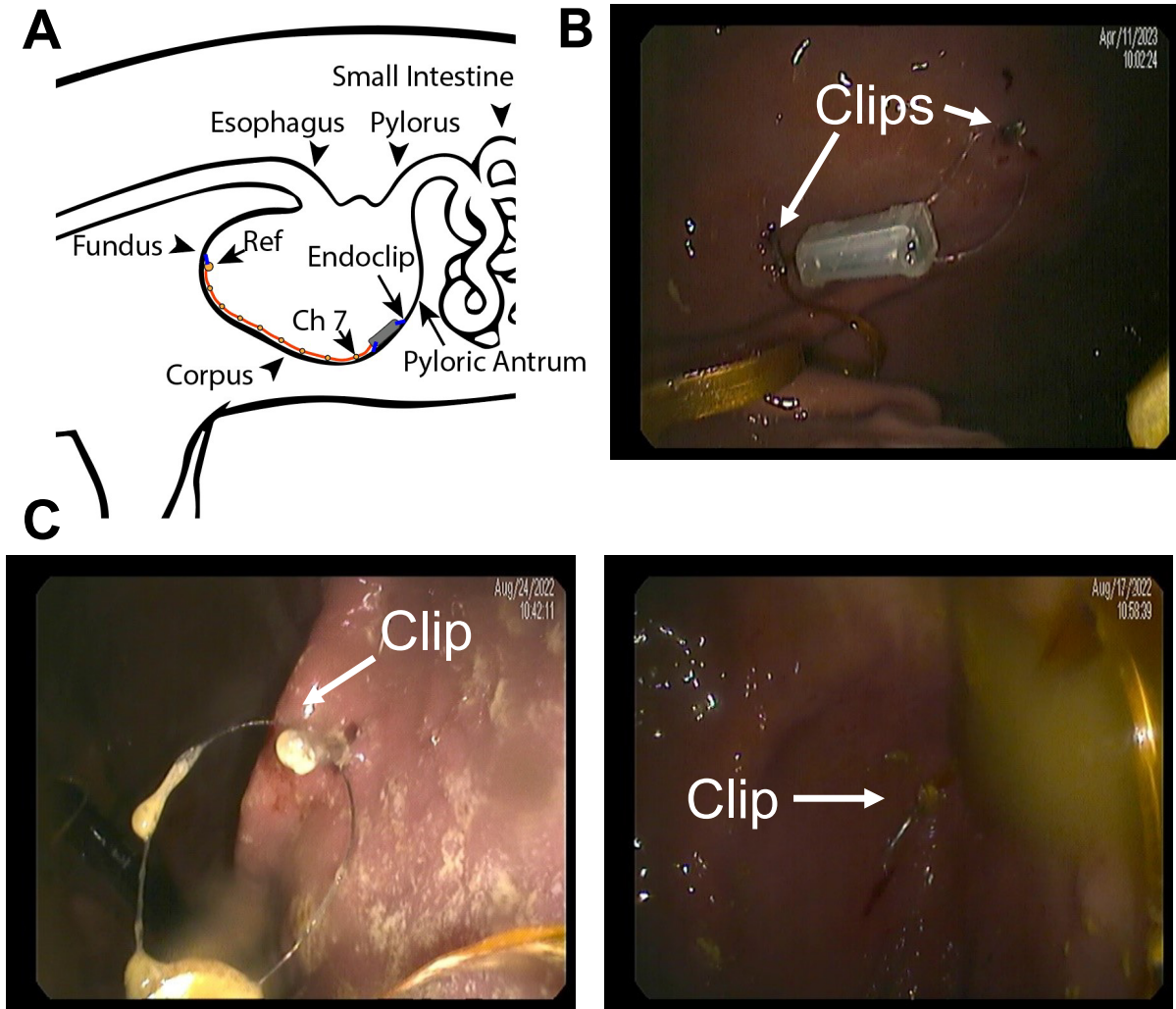
**Figure 4.1.1: Placement and retention for long term studies.** (A) Electrodes were placed along the greater curvature of the stomach with the reference electrode in the fundus and measurement electrodes along the corpus. (B) The capsule body was secured by two endoclips on either side, while (C) the reference electrode was secured by one clip via a nitinol wire.

## 4.2 Study Design and Device Reliability

After placement (in the mornings), the device would sleep until approximately noon and record for 45 minutes. The device was then programmed to sleep for 22 hours to capture recordings during different activities as outlined in Figure 4.2.1.
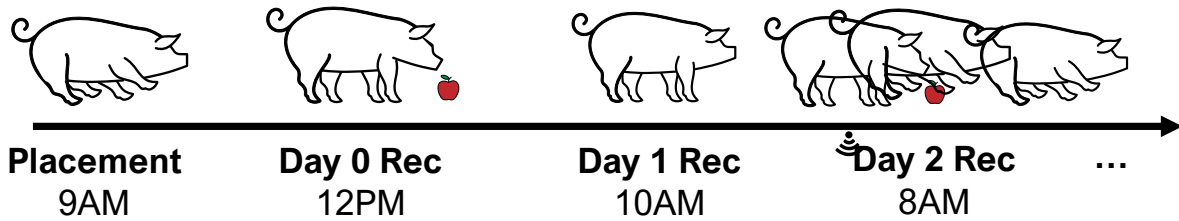
**Figure 4.2.1: Experiment flow.** MiGUT was configured to record during different times of day to capture different behaviors.

We observed over the course of four days the quality of the signal is consistent and of high quality (after which the device ran out of battery) as shown in Figure 4.2.2. While there are changes in signal amplitude, these are believed to be caused by changes in behavior discussed in the following section and not due to degradation of the electrodes or device. Additionally, no motion artifacts are observed during these long recording sessions. Select areas of high activity are shown in Figure 4.2.2 and can be seen to be smooth continuous changes in potential, and not similar to motion artifacts reported in literature [80]. This is transformational as motion artifacts have been a key limiting factor prevention adoption of gastric mapping systems [80], with signal processing algorithms developed specifically because of this to extract the underlying gastric signals [47].



**Figure 4.2.2: Data recorded over multiple days.** Day 0 the animal was eating during most of the recording session, Day 1 the animal was walking around while on liquid diet, Day 2 the animal on solid diet was ambulating, Day three the animal was on solid diet and resting.

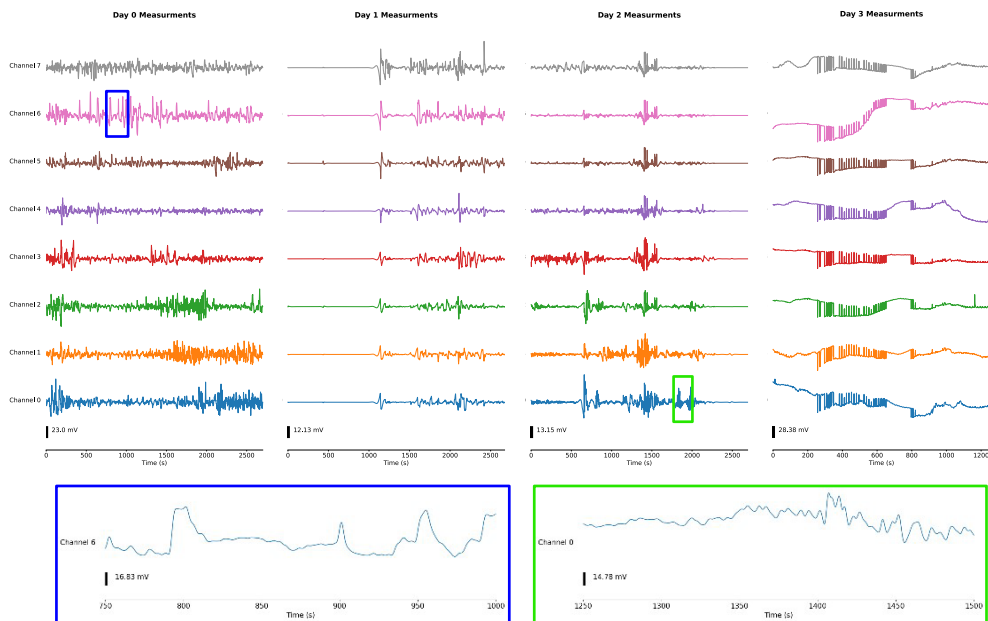This shows that MiGUT can be used reliably over multiple days, without any restrictions to the subjects' activities or diet. During the study, the pig was fed a combination of pellets, fruits, and vegetables, which did not interfere with any electrodes (all channels were able to obtain high quality measurements). Additionally, the peristaltic waves in the stomach did not dislodge the device. This showcases how MiGUT can be used for long term high quality recordings.

Fourteen studies were conducted, with one removed due to a poor ground connection (retention broke), and one the electrode broke during placement (large reference torn off in over tube). Different configurations were programmed to provide segmented data over multiple days as well as single continuous recordings for ~3 hours. In eight of the successful studies, a dominant frequency of 4.39cpm (SD: 0.27cpm) is observed.

## 4.3 Behavior Analysis

In six studies, 4.5 hours of video recordings were also taken simultaneously during recording sessions. At first, a GoPro (CA, USA; 1080p 30fps) was used but later studies used mounted 1080p HD IP cameras with night vision to enable recording without human influence present. This video was first labeled, with each frame of video associated with a behavior: feeding, ambulating, sleeping, or playing. Then, the timestamps were synchronized with the recorded electrophysiological signals from MiGUT. Figure 4.3.1 shows distinct changes in amplitude during different behaviors. Specifically the amplitude can be seen to be 3-6x larger when feeding compared to ambulation or resting, which is also seen in the frequency spectrum as a ~3.2x increase in power.
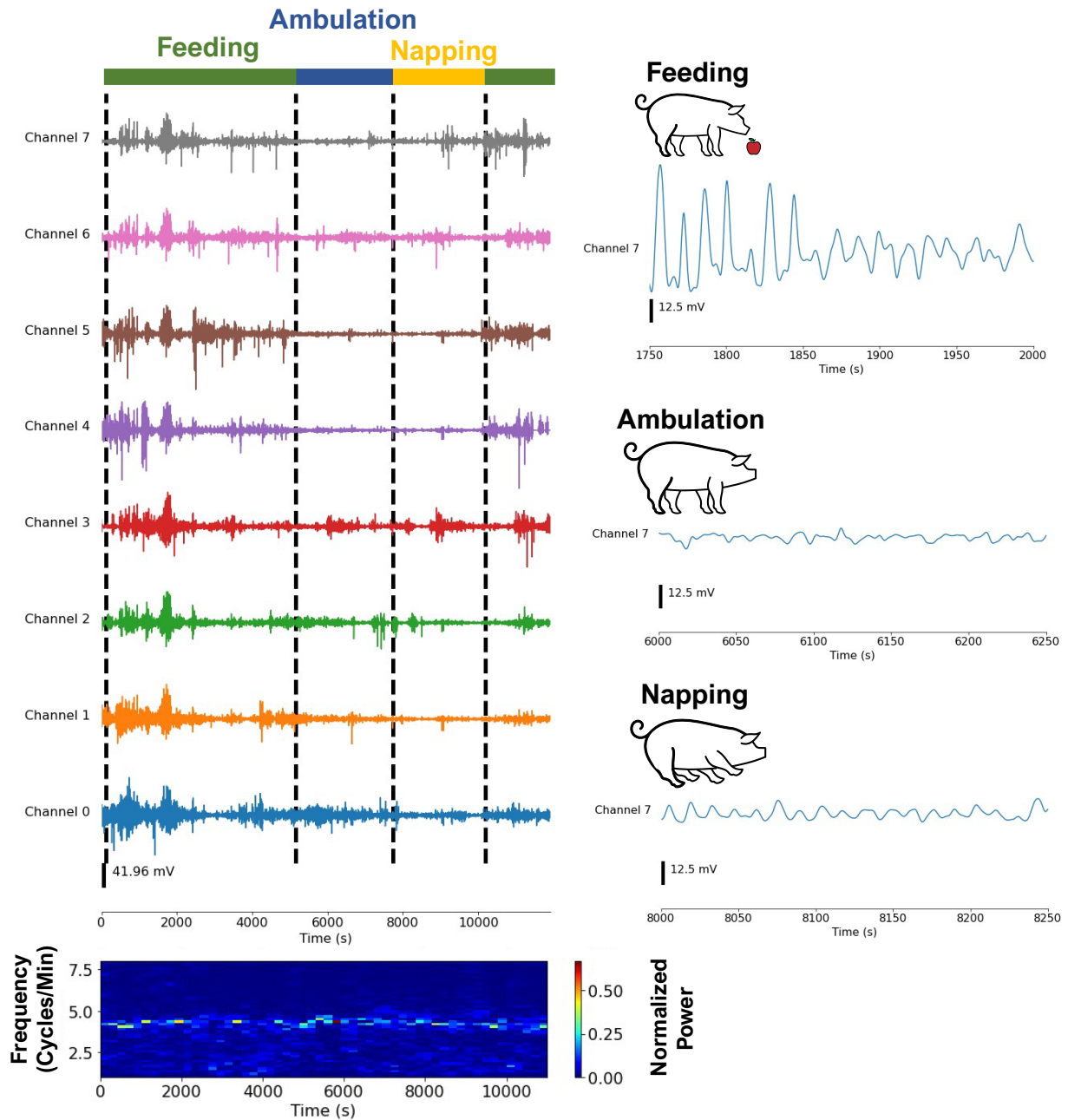
**Figure 4.3.1: Changes in Slow Wave by Behavior.** Filtered measurements shown with corresponding spectrogram, labeled with the associated behavior the pig was exhibiting. Zoom in shows a significantly increased amplitude during feeding when compared to ambulating or napping.

## 4.4 Passage Study

To validate this device could be safely implemented clinically, a passage study was conducted to ensure the device size (with long flexible electrodes) would not cause an

obstruction after measurements were obtained. For tracking purposes, a device without the electronics was filled with 3.5-4g of stainless steel powder (Sigma-Aldrich) matching the weight of MiGUT while ensuring clear visibility in X-Ray images. The largest electrode sizes, which had the thickest width along the ribbon, were used in these studies – smaller electrodes are hypothesized to pass easier. The modified device is shown in Figure 4.4.1B.
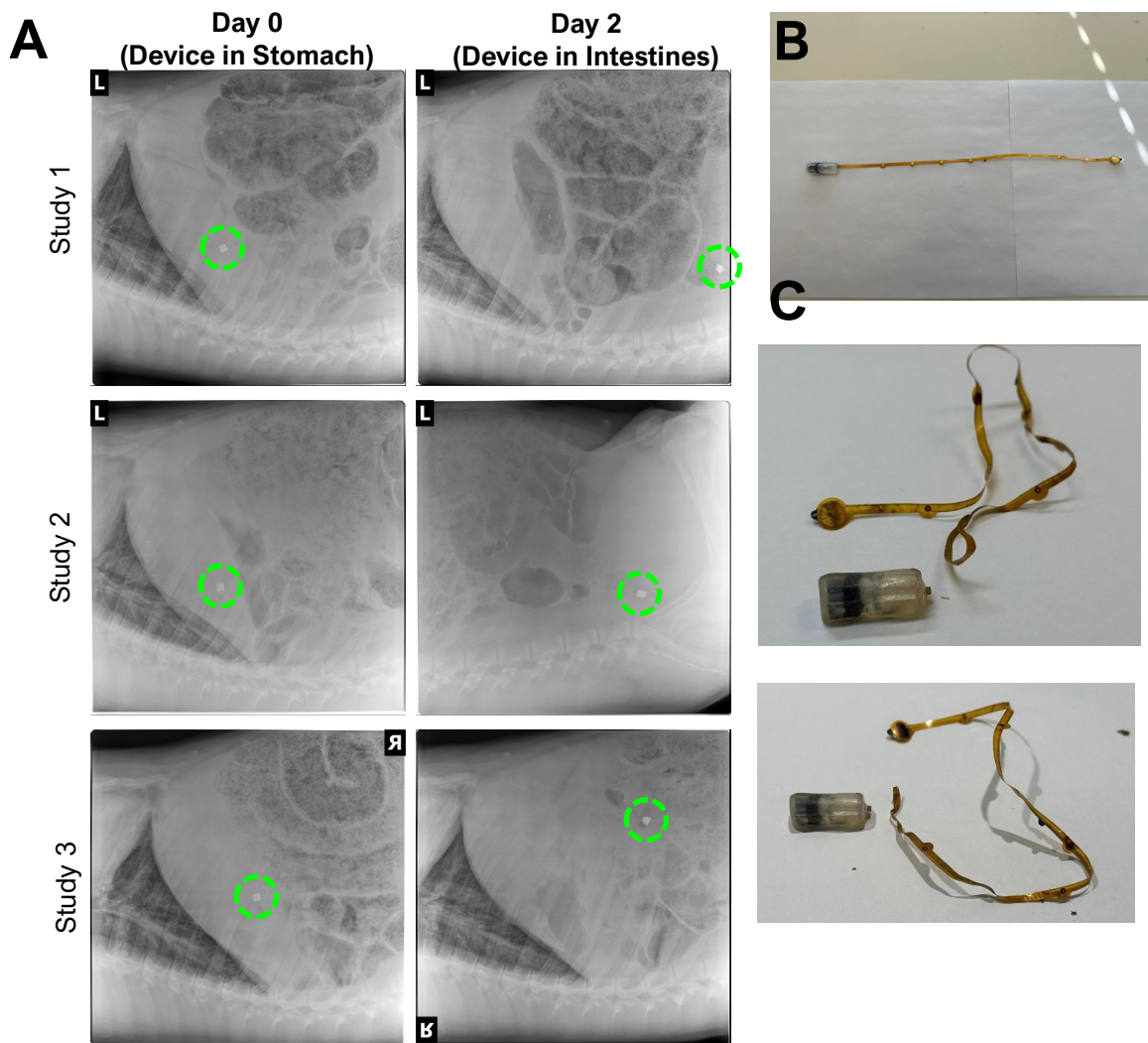


**Figure 4.4.1: Passage Study.** (A) X-Rays from device after it was placed on Day 0, and position at Day 2, device highlighted by green circle. (B) Dummy device before placement. (C) Dummy device after retrieval.

Over the course of three studies, all devices were shown to unroll in the stomach, passed into the intestines by day two, and were found excreted by day five (Figure 4.4.1A). One device was found to have the electrode torn off (Figure 4.4.1C), which is believed to have occurred after

excretion.  This suggests the device can pass without obstruction and does not pose a safety risk. Further disassembly methods or dissolvable electrodes are worth investigating for patient comfort.

# Chapter 5 Conclusion

## 5.1 Discussion

MiGUT is able to record high quality electrical signals from the gastric environment, including the gastric slow wave, heart rate, respiration rate, and other signals which require further study (possibly related to control of the migrating motor complex). Currently, this is believed to be the first ingestible device (in a swallowable formfactor) able to record from the mucosa over long periods of time, demonstrated in an awake, unrestricted pig. Our results generally match those reported in literature, however we report a slightly higher slow wave frequency (4.39cpm, N=8 ambulatory) compared to that reported in weaner pigs (3.2cpm [36], [73]) and humans (2.8cpm [22]), but lower than canine (5.2cpm [81]). In [36] this would be considered tachygastria, however as these results were consistent for long periods (>45min) we believe this increase in frequency could either be attributed with ingestion of a bolus (which typically occurred approximately one hour before each recording) or due to lack of anesthesia. While not previously studied in context of the enteric nervous system, the fed motor pattern is characterized by contractions of irregular amplitude and frequency which could be promoted by a natural increase in the slow wave frequency [21]. Similarly, as the migrating motor complex has been shown to decrease in frequency during sleep an interesting study would involve studying the impact of deep sleep on the slow wave [21]. All previous high resolution studies have been done with the animal anesthetized which could have also impacted the slow wave frequency during their experiments. Opioids, which are commonly used in anesthesia, have previously been seen to significantly decrease or completely suppress the slow wave frequency and power in 11/19 patients [82]. This may explain why our results from ambulating pigs are of higher frequency and higher amplitude than previously reported. MiGUT can enable more comprehensive studies to be conducted, continuously measuring before and during sedation.

MiGUT has also highlighted the variability in measurements that one might record from the stomach at different times. It has generally been considered that the slow wave is ever-present in the stomach [83], with superimposed rapid depolarizations from action potentials exceeding the threshold required to cause contractions [21]. This has been reported in several studies spanning multiple animals in anesthetized and conscious settings. Interestingly, we

observed times where no slow wave activity was seen, in two separate animals for 45 minutes recording sessions coinciding with the animals being on liquid diet. In days prior and after, post feeding the slow wave was recorded with in the same animals with the devices in the same position. During these periods of quiescence the heart rate signal and respiratory signals can still be observed as in the anesthetized experiments, suggesting this is not a device or contact issue. One possibility is that these recordings fell in phase I of the migrating motor complex, characterized by motor quiescence which can last up to 67 minutes in humans [21]. Studies of the migrating motor complex have shown "Microwaves" (<9 mmHg) at the same frequency of the slow wave [84], but these were performed during invasive surgeries possibly causing additional stimulation. Longer term studies with MiGUT will provide more insight into electrical correlations with the migrating motor complex, fed motor pattern, and reveal the extent of these electrically quiescence periods.

Lastly, the optimal placement of the device and electrode configuration is still a topic of active investigation. The most interesting and impactful parameter varied was the location of the reference electrode. Acute, invasive systems have used a wide range of references far away from the stomach to provide a stable reference, such as the surface of the abdomen [73], hind leg [85], in tissue bath [34], while ambulating tethered systems have typically used bi-polar electrodes [39]. MiGUT was positioned such that the reference was either placed in the corpus during anesthetized experiments or in the fundus during ambulating studies. Measurements taken referenced to the corpus were generally found to have a smaller variance over time compared to measurements referenced from the fundus, however other factors such as reference electrode clipping and different settings make it difficult to come to a clear conclusion. The fundus is believed to be the better choice as it naturally provides a stable, electrically quiet reference, but there may be an optimal distance from the measurement electrodes that would enable arbitrary placement (e.g. in the corpus) allowing for easier to implement electrode designs.

## 5.2 Future Work

MiGUT opens many avenues of exploration for neural recordings in the gut. The interchangeable electrodes will allow for further optimization and characterization of different electrode sizes and spacing, optimal reference location, and a platform to evaluate the quality of

recordings from electrodes with different retention mechanisms. Specifically it would be ideal to replace the endoclips used for retention with a mucoadhesive that provides a high quality electrical connection and secure each electrode for multiple days. In its current form, MiGUT enables a number of fundamental experiments to be done to better understand the enteric nervous system, slow wave, migrating motor complex, and fed motor pattern over long periods of time while not confined to a clinical setting. The size of the device would allow for multiple to be deployed at once if desired, allowing for simultaneous recordings throughout the GI tract. This could be especially useful when paired with disease models to better understand gastric neuropathies from an electrical perspective over long periods of time. Towards clinical translation, the next steps would involve a small re-design to accommodate the silver oxide batteries and further miniaturizing the size, which could be accomplished by using more advanced PCB manufacturing techniques or integrating all the components into a single custom integrated circuit.

MiGUT can also be used as a general purpose, ultra small neural acquisition system to assist with other studies. As an example, MiGUT could be used in combination with Gastric Electric Stimulators to better understand what the optimal parameters are with high resolution recordings. Later, by adding stimulation capabilities to MiGUT, gastric stimulation could be provided in a closed loop manner for additional power savings and personalized therapy. Other avenues of parallel measurements include behavioral analysis, anesthesia monitoring/recovery, and other brain-gut axis studies.

Finally, ingestible electronics represent the forefront of biomedical devices that are small, power efficient, and can survive harsh environments – fundamental challenges that can be translated to a number of other biomedical and smart devices. There is still much work to be done in battery technology to increase the power density, low power communications which can effectively communicate with devices deep within the body, and durable device packaging that can survive the gastric environment for an ultra long period of time. Immediate steps to overcome these challenges could involve wireless charging or energy harvesting, custom antenna designs, or on-device processing to limit communications. It is an exciting time to work on ingestible electronics with many future innovations to come.

# Bibliography

[1] A. D. Sperber *et al.*, "Worldwide Prevalence and Burden of Functional Gastrointestinal Disorders, Results of Rome Foundation Global Study," *Gastroenterology*, vol. 160, no. 1, pp. 99-114.e3, Jan. 2021, doi: 10.1053/j.gastro.2020.04.014.

[2] D. A. Drossman, "Functional Gastrointestinal Disorders: History, Pathophysiology, Clinical Features, and Rome IV," *Gastroenterology*, vol. 150, no. 6, pp. 1262-1279.e2, May 2016, doi: 10.1053/j.gastro.2016.02.032.

[3] A. Madisch, S. Miehlke, and J. Labenz, "Management of functional dyspepsia: Unsolved problems and new perspectives," *World J. Gastroenterol. WJG*, vol. 11, no. 42, pp. 6577–6581, Nov. 2005, doi: 10.3748/wjg.v11.i42.6577.

[4] M. Camilleri *et al.*, "Gastroparesis," *Nat. Rev. Dis. Primer*, vol. 4, no. 1, p. 41, Nov. 2018, doi: 10.1038/s41572-018-0038-z.

[5] M. Grover, G. Farrugia, and V. Stanghellini, "Gastroparesis: a turning point in understanding and treatment," *Gut*, vol. 68, no. 12, pp. 2238–2250, Dec. 2019, doi: 10.1136/gutjnl-2019-318712.

[6] T. L. Abell *et al.*, "Treatment of gastroparesis: a multidisciplinary clinical review," *Neurogastroenterol. Motil.*, vol. 18, no. 4, pp. 263–283, 2006, doi: 10.1111/j.1365-2982.2006.00760.x.

[7] J. B. Furness, "The enteric nervous system and neurogastroenterology," *Nat. Rev. Gastroenterol. Hepatol.*, vol. 9, no. 5, pp. 286–294, May 2012, doi: 10.1038/nrgastro.2012.32.

[8] A. B. Shreiner, J. Y. Kao, and V. B. Young, "The gut microbiome in health and in disease," *Curr. Opin. Gastroenterol.*, vol. 31, no. 1, pp. 69–75, Jan. 2015, doi: 10.1097/MOG.0000000000000139.

[9] W. C. ALVAREZ, "NEW METHODS OF STUDYING GASTRIC PERISTALSIS," *J. Am. Med. Assoc.*, vol. 79, no. 16, pp. 1281–1285, Oct. 1922, doi: 10.1001/jama.1922.02640160001001.

[10] K. L. Koch and R. M. Stern, *Handbook of electrogastrography*. New York: Oxford University Press, 2004.

[11] I. H. Tumpeer, "EFFECTS OF GASTRIC AND INTESTINAL HYPERPERISTALSIS ON THE ELECTROCARDIOGRAM AS DEMONSTRATED BY SIMULTANEOUS MECHANOGRAMS AND INDIRECT AND SEMIDIRECT ELECTRIC LEADS," *Ann. Intern. Med.*, vol. 10, no. 4, p. 487, Oct. 1936, doi: 10.7326/0003-4819-10-4-487.

[12] R. C. Davis, L. Garafolo, and F. P. Gault, "An exploration of abdominal potentials," *J. Comp. Physiol. Psychol.*, vol. 50, pp. 519–523, 1957, doi: 10.1037/h0048466.

[13] R. C. Davis, L. Garafolo, and K. Kveim, "Conditions associated with gastrointestinal activity," *J. Comp. Physiol. Psychol.*, vol. 52, pp. 466–475, 1959, doi: 10.1037/h0044130.

[14] M. A. Sobakin, I. P. Smirnov, and L. N. Mishin, "Electrogastrography," *IRE Trans. Bio-Med. Electron.*, vol. 9, no. 2, pp. 129–132, Apr. 1962, doi: 10.1109/TBMEL.1962.4322977.

[15] T. S. Nelsen and S. Kohatsu, "Clinical electrogastrography and its relationship to gastric surgery," *Am. J. Surg.*, vol. 116, no. 2, pp. 215–222, Aug. 1968, doi: 10.1016/0002-9610(68)90496-0.

[16] B. H. Brown, R. H. Smallwood, H. L. Duthie, and C. J. Stoddard, "Intestinal smooth muscle electrical potentials recorded from surface electrodes," *Med. Biol. Eng.*, vol. 13, no. 1, pp. 97–103, Jan. 1975, doi: 10.1007/BF02478194.

[17] R. H. Smallwood, "Analysis of gastric electrical signals from surface electrodes using phaselock techniques: Part 1—System design," *Med. Biol. Eng. Comput.*, vol. 16, no. 5, pp. 507–512, Sep. 1978, doi: 10.1007/BF02457800.

[18] R. M. Stern, K. L. Koch, W. R. Stewart, and M. W. Vasey, "Electrogastrography: Current Issues in Validation and Methodology," *Psychophysiology*, vol. 24, no. 1, pp. 55–64, 1987, doi: 10.1111/j.1469-8986.1987.tb01862.x.

[19] S. Kuruppu, L. K. Cheng, T. R. Angeli, R. Avci, and N. Paskaranandavadivel, "High-Resolution Mapping of Intestinal Spike Bursts and Motility," in *2020 42nd Annual International Conference of the IEEE Engineering in Medicine & Biology Society (EMBC)*, Jul. 2020, pp. 1779–1782. doi: 10.1109/EMBC44109.2020.9175879.

[20] J. E. Pandolfino and P. J. Kahrilas, "AGA technical review on the clinical use of esophageal manometry," *Gastroenterology*, vol. 128, no. 1, pp. 209–224, Jan. 2005, doi: 10.1053/j.gastro.2004.11.008.

[21] D. K. Podolsky, Ed., *Yamada's textbook of gastroenterology*, Sixth edition. Chichester, West Sussex ; Hoboken, NJ: John Wiley & Sons Inc, 2016.

[22] G. O'Grady *et al.*, "Origin and propagation of human gastric slow-wave activity defined by high-resolution mapping," *Am. J. Physiol.-Gastrointest. Liver Physiol.*, vol. 299, no. 3, pp. G585–G592, Sep. 2010, doi: 10.1152/ajpgi.00125.2010.

[23] N. Paskaranandavadivel *et al.*, "Ambulatory gastric mucosal slow wave recording for chronic experimental studies," in *2017 39th Annual International Conference of the IEEE Engineering in Medicine and Biology Society (EMBC)*, Jul. 2017, pp. 755–758. doi: 10.1109/EMBC.2017.8036934.

[24] Z. Y. Lin, R. W. McCallum, B. D. Schirmer, and J. D. Z. Chen, "Effects of pacing parameters on entrainment of gastric slow waves in patients with gastroparesis," *Am. J. Physiol.-Gastrointest. Liver Physiol.*, vol. 274, no. 1, pp. G186–G191, Jan. 1998, doi: 10.1152/ajpgi.1998.274.1.G186.

[25] B. O. Familoni, T. L. Abell, G. Voeller, A. Salem, and O. Gaber, "Electrical Stimulation at a Frequency Higher than Basal Rate in Human Stomach," *Dig. Dis. Sci.*, vol. 42, no. 5, 1997.

[26] Z. Lin, I. Sarosiek, J. Forster, I. Damjanov, Q. Hou, and R. W. Mccallum, "Association of the status of interstitial cells of Cajal and electrogastrogram parameters, gastric emptying and symptoms in patients with gastroparesis," *Neurogastroenterol. Motil.*, vol. 22, no. 1, pp. 56-e10, 2010, doi: 10.1111/j.1365-2982.2009.01365.x.

[27] H. P. Parkman, W. L. Hasler, J. L. Barnett, and E. Y. Eaker, "Electrogastrography: a document prepared by the gastric section of the American Motility Society Clinical GI Motility Testing Task Force," *Neurogastroenterol. Motil.*, vol. 15, no. 2, pp. 89–102, 2003, doi: 10.1046/j.1365-2982.2003.00396.x.

[28] G. O'Grady *et al.*, "Abnormal Initiation and Conduction of Slow-Wave Activity in Gastroparesis, Defined by High-Resolution Electrical Mapping," *Gastroenterology*, vol. 143, no. 3, pp. 589-598.e3, Sep. 2012, doi: 10.1053/j.gastro.2012.05.036.

[29] R. A. Travagli, K. N. Browning, and M. Camilleri, "Parkinson disease and the gut: new insights into pathogenesis and clinical relevance," *Nat. Rev. Gastroenterol. Hepatol.*, vol. 17, no. 11, pp. 673–685, Nov. 2020, doi: 10.1038/s41575-020-0339-z.

[30] J. D. Jones, E. Rahmani, E. Garcia, and J. P. Jacobs, "Gastrointestinal symptoms are predictive of trajectories of cognitive functioning in de novo Parkinson's disease," *Parkinsonism Relat. Disord.*, vol. 72, pp. 7–12, Mar. 2020, doi: 10.1016/j.parkreldis.2020.01.009.

[31] T. Warnecke, K.-H. Schäfer, I. Claus, K. Del Tredici, and W. H. Jost, "Gastrointestinal involvement in Parkinson's disease: pathophysiology, diagnosis, and management," *NPJ Park. Dis.*, vol. 8, p. 31, Mar. 2022, doi: 10.1038/s41531-022-00295-x.

[32] E. Y. Hsiao, "Gastrointestinal Issues in Autism Spectrum Disorder," *Harv. Rev. Psychiatry*, vol. 22, no. 2, pp. 104–111, Apr. 2014, doi: 10.1097/HRP.0000000000000029.

[33] V. Saurman, K. G. Margolis, and R. A. Luna, "Autism Spectrum Disorder as a Brain-Gut-Microbiome Axis Disorder," *Dig. Dis. Sci.*, vol. 65, no. 3, pp. 818–828, Mar. 2020, doi: 10.1007/s10620-020-06133-5.

[34] W. J. Lammers, A. al-Kais, S. Singh, K. Arafat, and T. Y. el-Sharkawy, "Multielectrode mapping of slow-wave activity in the isolated rabbit duodenum," *J. Appl. Physiol.*, vol. 74, no. 3, pp. 1454–1461, Mar. 1993, doi: 10.1152/jappl.1993.74.3.1454.

[35] G. O'Grady *et al.*, "A comparison of gold versus silver electrode contacts for high-resolution gastric electrical mapping using flexible printed circuit board arrays," *Physiol. Meas.*, vol. 32, no. 3, pp. N13–N22, Mar. 2011, doi: 10.1088/0967-3334/32/3/N02.

[36] J. U. Egbuji *et al.*, "Origin, propagation and regional characteristics of porcine gastric slow wave activity determined by high-resolution mapping," *Neurogastroenterol. Motil.*, vol. 22, no. 10, pp. e292–e300, 2010, doi: 10.1111/j.1365-2982.2010.01538.x.

[37] T. R. Angeli *et al.*, "High-resolution electrical mapping of porcine gastric slow-wave propagation from the mucosal surface," *Neurogastroenterol. Motil.*, vol. 29, no. 5, p. e13010, 2017, doi: 10.1111/nmo.13010.

[38] G. O'Grady *et al.*, "Methods for High-Resolution Electrical Mapping in the Gastrointestinal Tract," *IEEE Rev. Biomed. Eng.*, vol. 12, pp. 287–302, 2019, doi: 10.1109/RBME.2018.2867555.

[39] N. Paskaranandavadivel *et al.*, "Multi-day, multi-sensor ambulatory monitoring of gastric electrical activity," *Physiol. Meas.*, vol. 40, no. 2, p. 025011, Mar. 2019, doi: 10.1088/1361-6579/ab0668.

[40] J. D. Chen, B. D. Schirmer, and R. W. McCallum, "Serosal and cutaneous recordings of gastric myoelectrical activity in patients with gastroparesis," *Am. J. Physiol.-Gastrointest. Liver Physiol.*, vol. 266, no. 1, pp. G90–G98, Jan. 1994, doi: 10.1152/ajpgi.1994.266.1.G90.

[41] R. Wang *et al.*, "A Miniature Configurable Wireless System for Recording Gastric Electrophysiological Activity and Delivering High-Energy Electrical Stimulation," *IEEE J. Emerg. Sel. Top. Circuits Syst.*, vol. 8, no. 2, pp. 221–229, Jun. 2018, doi: 10.1109/JETCAS.2018.2812105.

[42] N. Paskaranandavadivel, R. Wang, S. Sathar, G. O'Grady, L. K. Cheng, and A. Farajidavar, "Multi-channel wireless mapping of gastrointestinal serosal slow wave propagation," *Neurogastroenterol. Motil.*, vol. 27, no. 4, pp. 580–585, Apr. 2015, doi: 10.1111/nmo.12515.

[43] A. Javan-Khoshkholgh, J. C. Sassoon, and A. Farajidavar, "A Wireless Rechargeable Implantable System for Monitoring and Pacing the Gut in Small Animals," in *2019 IEEE Biomedical Circuits and Systems Conference (BioCAS)*, Nara, Japan: IEEE, Oct. 2019, pp. 1–4. doi: 10.1109/BIOCAS.2019.8919125.

[44] A. Ibrahim, M. Kiani, and A. Farajidavar, "A 64-channel wireless implantable system-on-chip for gastric electrical-wave recording," in *2016 IEEE SENSORS*, Orlando, FL, USA: IEEE, Oct. 2016, pp. 1–3. doi: 10.1109/ICSENS.2016.7808742.

[45] H. Liang, Z. Lin, and R. W. McCallum, "Artifact reduction in electrogastrogram based on empirical mode decomposition method," *Med. Biol. Eng. Comput.*, vol. 38, no. 1, pp. 35–41, Jan. 2000, doi: 10.1007/BF02344686.

[46] J. Yin and J. D. Z. Chen, "Electrogastrography: Methodology, Validation and Applications," *J. Neurogastroenterol. Motil.*, vol. 19, no. 1, pp. 5–17, Jan. 2013, doi: 10.5056/jnm.2013.19.1.5.

[47] A. A. Gharibans, B. L. Smarr, D. C. Kunkel, L. J. Kriegsfeld, H. M. Mousa, and T. P. Coleman, "Artifact Rejection Methodology Enables Continuous, Noninvasive Measurement of Gastric Myoelectric Activity in Ambulatory Subjects," *Sci. Rep.*, vol. 8, p. 5019, Mar. 2018, doi: 10.1038/s41598-018-23302-9.

[48] D. A. Carson, G. O'Grady, P. Du, A. A. Gharibans, and C. N. Andrews, "Body surface mapping of the stomach: New directions for clinically evaluating gastric electrical activity," *Neurogastroenterol. Motil.*, vol. 33, no. 3, p. e14048, 2021, doi: 10.1111/nmo.14048.

[49] A. S. Agrusa, A. B. Allegra, D. C. Kunkel, and T. P. Coleman, "Robust Methods to Detect Abnormal Initiation in the Gastric Slow Wave from Cutaneous Recordings," in *2020 42nd Annual International Conference of the IEEE Engineering in Medicine & Biology Society (EMBC)*, Jul. 2020, pp. 225–231. doi: 10.1109/EMBC44109.2020.9176634.

[50] R. Muñoz *et al.*, "Importance of Routine Preoperative Upper GI Endoscopy: Why All Patients Should Be Evaluated?," *Obes. Surg.*, vol. 19, no. 4, pp. 427–431, Apr. 2009, doi: 10.1007/s11695-008-9673-x.

[51] J.-M. Yang *et al.*, "Simultaneous functional photoacoustic and ultrasonic endoscopy of internal organs in vivo," *Nat. Med.*, vol. 18, no. 8, pp. 1297–1302, Aug. 2012, doi: 10.1038/nm.2823.

[52] M. H. Mellow and H. Pinkas, "Endoscopic Laser Therapy for Malignancies Affecting the Esophagus and Gastroesophageal Junction: Analysis of Technical and Functional Efficacy," *Arch. Intern. Med.*, vol. 145, no. 8, pp. 1443–1446, Aug. 1985, doi: 10.1001/archinte.1985.00360080117017.

[53] L. B. Cohen *et al.*, "AGA Institute Review of Endoscopic Sedation," *Gastroenterology*, vol. 133, no. 2, pp. 675–701, Aug. 2007, doi: 10.1053/j.gastro.2007.06.002.

[54] R. Eliakim *et al.*, "Prospective multicenter performance evaluation of the second-generation colon capsule compared with colonoscopy," *Endoscopy*, vol. 41, no. 12, pp. 1026–1031, Dec. 2009, doi: 10.1055/s-0029-1215360.

[55] K. Kalantar-Zadeh *et al.*, "A human pilot trial of ingestible electronic capsules capable of sensing different gases in the gut," *Nat. Electron.*, vol. 1, no. 1, pp. 79–87, Jan. 2018, doi: 10.1038/s41928-017-0004-x.

[56] M. Mimee *et al.*, "An ingestible bacterial-electronic system to monitor gastrointestinal health," *Science*, vol. 360, no. 6391, pp. 915–918, May 2018, doi: 10.1126/science.aas9315.

[57] C. Steiger, A. Abramson, P. Nadeau, A. P. Chandrakasan, R. Langer, and G. Traverso, "Ingestible electronics for diagnostics and therapy," *Nat. Rev. Mater.*, vol. 4, no. 2, pp. 83–98, Feb. 2019, doi: 10.1038/s41578-018-0070-3.

[58] E. De la Paz *et al.*, "A self-powered ingestible wireless biosensing system for real-time in situ monitoring of gastrointestinal tract metabolites," *Nat. Commun.*, vol. 13, no. 1, p. 7405, Dec. 2022, doi: 10.1038/s41467-022-35074-y.

[59] B. F. Cox *et al.*, "Ultrasound capsule endoscopy: sounding out the future," *Ann. Transl. Med.*, vol. 5, no. 9, pp. 201–201, May 2017, doi: 10.21037/atm.2017.04.21.

[60] K. B. Ramadi *et al.*, "Bioinspired, ingestible electroceutical capsules for hunger-regulating hormone modulation," *Sci. Robot.*, vol. 8, no. 77, p. eade9676, Apr. 2023, doi: 10.1126/scirobotics.ade9676.

[61] D. M. Bass, M. Prevo, and D. S. Waxman, "Gastrointestinal Safety of an Extended-Release, Nondeformable, Oral Dosage Form (OROS??)*: A Retrospective Study," *Drug Saf.*, vol. 25, no. 14, pp. 1021–1033, 2002, doi: 10.2165/00002018-200225140-00004.

[62] F. Li *et al.*, "Retention of the capsule endoscope: a single-center experience of 1000 capsule endoscopy procedures," *Gastrointest. Endosc.*, vol. 68, no. 1, pp. 174–180, Jul. 2008, doi: 10.1016/j.gie.2008.02.037.

[63] K. E. Blaho, K. S. Merigian, S. L. Winbery, L. J. Park, and M. Cockrell, "Foreign Body Ingestions in the Emergency Department: Case Reports and Review of Treatment," *J. Emerg. Med.*, vol. 16, no. 1, pp. 21–26, Jan. 1998, doi: 10.1016/S0736-4679(97)00229-1.

[64] D. C. Bock, A. C. Marschilok, K. J. Takeuchi, and E. S. Takeuchi, "Batteries used to power implantable biomedical devices," *Electrochimica Acta*, vol. 84, pp. 155–164, Dec. 2012, doi: 10.1016/j.electacta.2012.03.057.

[65] S.-Y. Yang *et al.*, "Powering Implantable and Ingestible Electronics," *Adv. Funct. Mater.*, vol. 31, no. 44, p. 2009289, 2021, doi: 10.1002/adfm.202009289.

[66] A. Alanaz and Y. Mohammedali, "Estimation of E-Field inside Muscle Tissue at MICS and ISM Frequencies Using Analytic and Numerical Methods," *Int. J. Biomed. Eng. Technol.*, vol. 2, pp. 29–33, May 2014, doi: 10.12691/jbet-2-3-1.

[67] S. Sharma *et al.*, "Location-aware ingestible microdevices for wireless monitoring of gastrointestinal dynamics," *Nat. Electron.*, Feb. 2023, doi: 10.1038/s41928-023-00916-0.

[68] M. A. Kwiatek *et al.*, "Quantification of distal antral contractile motility in healthy human stomach with magnetic resonance imaging," *J. Magn. Reson. Imaging*, vol. 24, no. 5, pp. 1101–1109, 2006, doi: 10.1002/jmri.20738.

[69] S. Hosseini, R. Avci, N. Paskaranandavadivel, V. Suresh, and L. K. Cheng, "Quantification of the Regional Properties of Gastric Motility using Dynamic Magnetic Resonance Images," *IEEE Open J. Eng. Med. Biol.*, pp. 1–7, 2023, doi: 10.1109/OJEMB.2023.3261224.

[70] A. C. Johnson, T. Louwies, C. O. Ligon, and B. Greenwood-Van Meerveld, "Enlightening the frontiers of neurogastroenterology through optogenetics," *Am. J. Physiol.-Gastrointest. Liver Physiol.*, vol. 319, no. 3, pp. G391–G399, Sep. 2020, doi: 10.1152/ajpgi.00384.2019.

[71] A. Pal, K. Indireshkumar, W. Schwizer, B. Abrahamsson, M. Fried, and J. G. Brasseur, "Gastric Flow and Mixing Studied Using Computer Simulation," *Proc. Biol. Sci.*, vol. 271, no. 1557, pp. 2587–2594, 2004.

[72] H.-W. Huang *et al.*, "An automated all-in-one system for carbohydrate tracking, glucose monitoring, and insulin delivery," *J. Controlled Release*, vol. 343, pp. 31–42, Mar. 2022, doi: 10.1016/j.jconrel.2022.01.001.

[73] P. Du *et al.*, "High-resolution Mapping of In Vivo Gastrointestinal Slow Wave Activity Using Flexible Printed Circuit Board Electrodes: Methodology and Validation," *Ann. Biomed. Eng.*, vol. 37, no. 4, pp. 839–846, Apr. 2009, doi: 10.1007/s10439-009-9654-9.

[74] Y. Jeon *et al.*, "Secure and Stable Wireless Communication for an Ingestible Device," presented at the EMBC, Australia: IEEE, 2023.

[75] T. C. Wang *et al.*, Eds., "Yamada's Textbook of Gastroenterology," in *Yamada's Textbook of Gastroenterology*, 1st ed.Wiley, 2022. doi: 10.1002/9781119600206.fmatter1.

[76] G. J. Sanger and J. B. Furness, "Ghrelin and motilin receptors as drug targets for gastrointestinal disorders," *Nat. Rev. Gastroenterol. Hepatol.*, vol. 13, no. 1, pp. 38–48, Jan. 2016, doi: 10.1038/nrgastro.2015.163.

[77] P. L. Ponugoti and D. K. Rex, "Clip retention rates and rates of residual polyp at the base of retained clips on colorectal EMR sites," *Gastrointest. Endosc.*, vol. 85, no. 3, pp. 530–534, Mar. 2017, doi: 10.1016/j.gie.2016.07.037.

[78] P. Saxena *et al.*, "Which Clip? A Prospective Comparative Study of Retention Rates of Endoscopic Clips on Normal Mucosa and Ulcers in a Porcine Model," *Saudi J. Gastroenterol.*, vol. 20, no. 6, p. 360, Dec. 2014, doi: 10.4103/1319-3767.145328.

[79] G. Donatelli *et al.*, "Closure of gastrointestinal defects with Ovesco clip: long-term results and clinical implications," *Ther. Adv. Gastroenterol.*, vol. 9, no. 5, pp. 713–721, Sep. 2016, doi: 10.1177/1756283X16652325.

[80] O. Bayguinov, G. W. Hennig, and K. M. Sanders, "Movement based artifacts may contaminate extracellular electrical recordings from GI muscles," *Neurogastroenterol. Motil.*, vol. 23, no. 11, pp. 1029-e498, 2011, doi: 10.1111/j.1365-2982.2011.01784.x.

[81] "Origin and propagation of the slow wave in the canine stomach: the outlines of a gastric conduction system." https://journals.physiology.org/doi/epdf/10.1152/ajpgi.90581.2008 (accessed Apr. 29, 2023).

[82] J. Walldén, G. Lindberg, M. Sandin, S.-E. Thörn, and M. Wattwil, "Effects of fentanyl on gastric myoelectrical activity: a possible association with polymorphisms of the μ-opioid receptor gene?," *Acta Anaesthesiol. Scand.*, vol. 52, no. 5, pp. 708–715, 2008, doi: 10.1111/j.1399-6576.2008.01624.x.

[83] W. E. Waterfall, H. L. Duthie, and B. H. Brown, "The electrical and motor actions of gastrointestinal hormones on the duodenum in man," *Gut*, vol. 14, no. 9, pp. 689–696, Sep. 1973, doi: 10.1136/gut.14.9.689.

[84] J. M. Collard and R. Romagnoli, "Human stomach has a recordable mechanical activity at a rate of about three cycles/minute," *Eur. J. Surg.*, vol. 166, no. 12, pp. 942–948, 2000, doi: 10.1080/110241500447100.

[85] P. Du *et al.*, "Automated detection of gastric slow wave events and estimation of propagation velocity vector fields from serosal high-resolution mapping," *Conf. Proc. Annu. Int. Conf. IEEE Eng. Med. Biol. Soc. IEEE Eng. Med. Biol. Soc. Conf.*, vol. 2009, pp. 2527–2530, 2009, doi: 10.1109/IEMBS.2009.5334822.
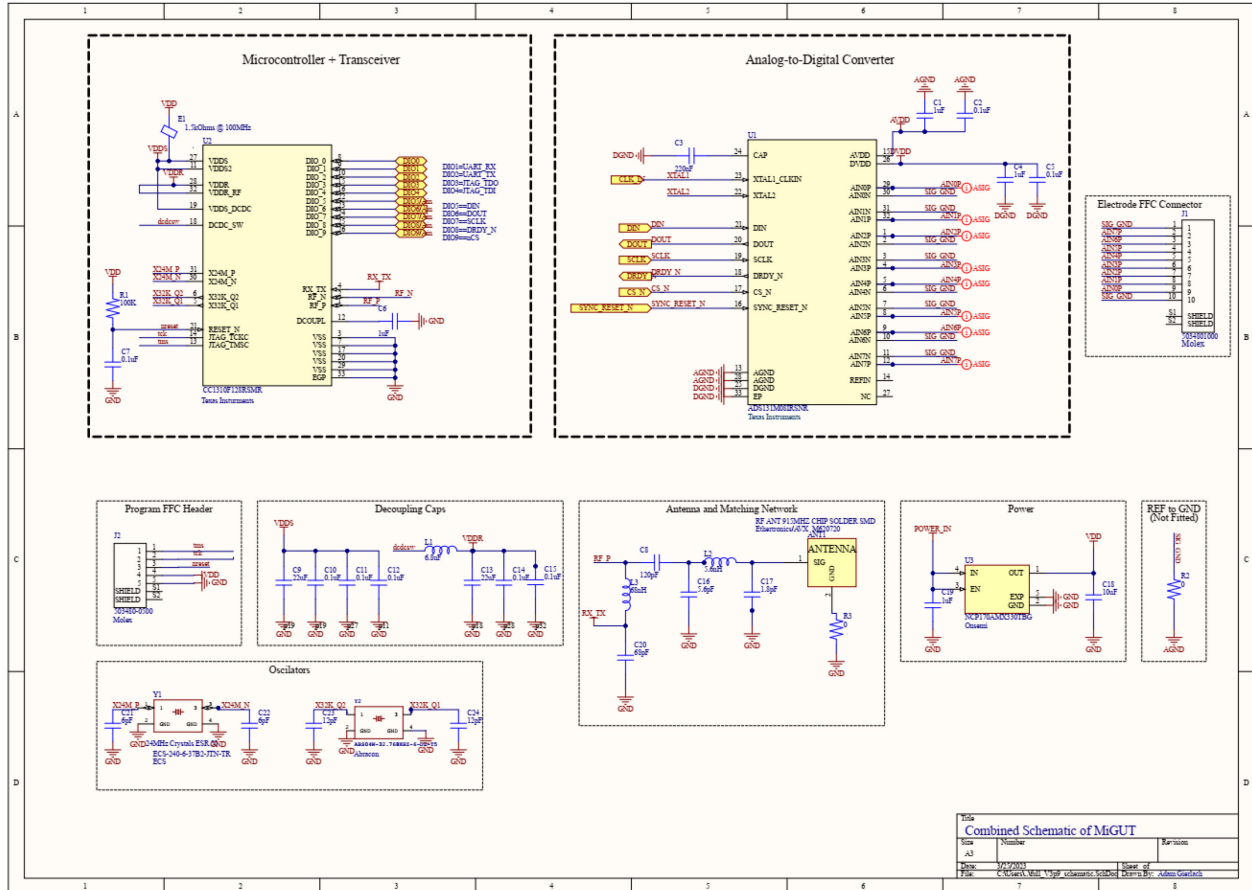
# Appendix

## A.1 Detailed schematic of MiGUT electronics



Figure A.1: Detailed schematic of MiGUT electronics.